PRUNE2 is a human prostate cancer suppressor regulated by the intronic long noncoding RNA *PCA3*

Ahmad Salameh[a,b,1], Alessandro K. Lee[a,1,2], Marina Cardó-Vila[a,c,d,e], Diana N. Nunes[a,f], Eleni Efstathiou[a,g], Fernanda I. Staquicini[a,c,d,e], Andrey S. Dobroff[a,c,d,e], Serena Marchiò[h], Nora M. Navone[a,g], Hitomi Hosoya[a,3], Richard C. Lauer[c,e,i], Sijin Wen[j,4], Carolina C. Salmeron[a,c,d,e], Anh Hoang[a,g], Irene Newsham[a], Leandro A. Lima[f], Dirce M. Carraro[f], Salvatore Oliviero[k], Mikhail G. Kolonin[b], Richard L. Sidman[l], Kim-Anh Do[j], Patricia Troncoso[a,m], Christopher J. Logothetis[a,g], Ricardo R. Brentani[f,5], George A. Calin[n,o], Webster K. Cavenee[p,6], Emmanuel Dias-Neto[a,f,q,6,7], Renata Pasqualini[a,c,d,e,g,6,7], and Wadih Arap[a,c,e,g,i,6,7]

[a]David H. Koch Center for Applied Research of Genitourinary Cancers, The University of Texas M.D. Anderson Cancer Center, Houston, TX 77030; [b]Brown Foundation Institute of Molecular Medicine, University of Texas Health Science Center at Houston, Houston, TX 77030; [c]University of New Mexico Cancer Center, University of New Mexico School of Medicine, Albuquerque, NM 87131; [d]Division of Molecular Medicine, University of New Mexico School of Medicine, Albuquerque, NM 87131; [e]Department of Internal Medicine, University of New Mexico School of Medicine, Albuquerque, NM 87131; [f]International Research Center, A.C. Camargo Cancer Center, São Paulo, SP 01508-010 Brazil; [g]Department of Genitourinary Medical Oncology, The University of Texas M.D. Anderson Cancer Center, Houston, TX 77030; [h]Candiolo Cancer Institute and Department of Oncology, University of Turin, Candiolo 10060, Italy; [i]Division of Hematology/Oncology, University of New Mexico School of Medicine, Albuquerque, NM 87131; [j]Department of Biostatistics, The University of Texas M.D. Anderson Cancer Center, Houston, TX 77030; [k]Human Genetics Foundation, Torino 10126, Italy; [l]Harvard Medical School and Department of Neurology, Beth Israel Deaconess Medical Center, Boston, MA 02215; [m]Department of Pathology, The University of Texas M.D. Anderson Cancer Center, Houston, TX 77030; [n]Department of Experimental Therapeutics, The University of Texas M.D. Anderson Cancer Center, Houston, TX 77030; [o]Center for RNA Interference and Noncoding RNA, The University of Texas M.D. Anderson Cancer Center, Houston, TX 77030; [p]Ludwig Institute for Cancer Research, University of California-San Diego, La Jolla, CA 92093; and [q]Institute of Psychiatry, University of São Paulo Medical School, São Paulo 01060, Brazil

Edited by Owen N. Witte, Howard Hughes Medical Institute, University of California, Los Angeles, CA, and approved May 13, 2015 (received for review March 16, 2015)

***Prostate cancer antigen 3* (*PCA3*) is the most specific prostate cancer biomarker but its function remains unknown. Here we identify *PRUNE2*, a target protein-coding gene variant, which harbors the *PCA3* locus, thereby classifying *PCA3* as an antisense intronic long noncoding (lnc)RNA. We show that *PCA3* controls PRUNE2 levels via a unique regulatory mechanism involving formation of a *PRUNE2/PCA3* double-stranded RNA that undergoes adenosine deaminase acting on RNA (ADAR)-dependent adenosine-to-inosine RNA editing. *PRUNE2* expression or silencing in prostate cancer cells decreased and increased cell proliferation, respectively. Moreover, *PRUNE2* and *PCA3* elicited opposite effects on tumor growth in immunodeficient tumor-bearing mice. Coregulation and RNA editing of *PRUNE2* and *PCA3* were confirmed in human prostate cancer specimens, supporting the medical relevance of our findings. These results establish *PCA3* as a dominant-negative oncogene and *PRUNE2* as an unrecognized tumor suppressor gene in human prostate cancer, and their regulatory axis represents a unique molecular target for diagnostic and therapeutic intervention.**

PRUNE2 | *PCA3* | long noncoding RNA | ADAR | prostate cancer

Several lines of evidence demonstrate that long noncoding RNAs (lncRNAs) are functional in carcinogenesis through regulatory mechanisms such as promoter looping, alternative splicing, antisense gene silencing, transcriptional regulation, and DNA repair, thus potentially serving as tumor markers. A few lncRNA species have emerged as potential prostate cancer biomarkers such as *prostate cancer gene expression marker-1* (*PCGEM1*) and *prostate cancer noncoding RNA1* (*PRNCR1*), which enhance androgen receptor (AR)-dependent gene activation, and *prostate cancer-associated ncRNA transcript-1* (*PCAT1*), which silences *BRCA2* via posttranscriptional homologous recombination (1). Notably, the most specific biomarker in human prostate cancer identified to date is an lncRNA, *prostate cancer antigen 3* (*PCA3*, also known as $PCA3^{DD3}$ or $DD3^{PCA3}$), which is up-regulated in human prostate cancer (2). Since its discovery more than 15 y ago, *PCA3* has been extensively investigated (3) and has been approved for clinical applications to aid the diagnosis of prostate cancer in both the European Union and the United States. Paradoxically—despite its striking clinical specificity—the inherent cellular role of the lncRNA *PCA3* in human prostate cancer, if any, remains completely unknown (1). Here we report a unique biological function for *PCA3*. Within a single functional genetic unit, we show that *PCA3* is an antisense intronic lncRNA that down-regulates an as yet unrecognized tumor suppressor gene, a human homolog of the *Drosophila* prune gene, *PRUNE2*, through a process that involves RNA editing mediated by a supramolecular complex containing adenosine deaminase acting on RNA (ADAR) family members. We propose a working model in which *PCA3* acts as a dominant-negative oncogene in prostate cancer and show consistent results in therapeutic preclinical models and in patient-derived human samples. Therefore, the molecular interaction of *PRUNE2* and *PCA3* is a candidate target for translational applications.

Results

***PCA3* Is an Antisense Intronic lncRNA Within a Single *PRUNE2* Transcriptional Unit.** Certain mammalian lncRNAs are embedded in the intronic-antisense regions of protein-coding genes (4–6).

Author contributions: A.S., A.K.L., M.C.-V., D.N.N., E.E., F.I.S., A.S.D., E.D.-N., R.P., and W.A. designed research; A.S., A.K.L., M.C.-V., D.N.N., F.I.S., A.S.D., H.H., A.H., and E.D.-N. performed research; E.E., S.M., N.M.N., R.C.L., S.W., C.C.S., D.M.C., S.O., M.G.K., R.L.S., K.-A.D., P.T., C.J.L., R.R.B., and G.A.C. contributed new reagents/analytic tools; A.S., A.K.L., M.C.-V., D.N.N., E.E., F.I.S., A.S.D., H.H., R.C.L., S.W., C.C.S., I.N., L.A.L., M.G.K., R.L.S., K.-A.D., P.T., C.J.L., R.R.B., G.A.C., W.K.C., E.D.-N., R.P., and W.A. analyzed data; A.S., A.K.L., M.C.-V., D.N.N., E.E., F.I.S., A.S.D., R.L.S., G.A.C., W.K.C., E.D.-N., R.P., and W.A. wrote the paper; and E.D.-N., R.P., and W.A. jointly supervised this project.

Conflict of interest statement: The University of New Mexico has filed patents on the technology and intellectual property reported here. If licensing or commercialization occurs, the researchers (A.S., A.K.L., D.N.N., E.D.-N., R.P., and W.A.) are entitled to standard royalties.

This article is a PNAS Direct Submission.

Freely available online through the PNAS open access option.

Data deposition: The sequences reported in this paper have been deposited in the GenBank database (accession nos. FJ808772, FJ808773, and AF103907).

[1]A.S. and A.K.L. contributed equally to this work.

[2]Present address: Janssen-Cilag SpA., Cologno Monzese, Milan 20093, Italy.

[3]Present address: The US Naval Hospital Yokosuka, PSC 475 FPO AP 96350-9998, Japan.

[4]Present address: School of Public Health, West Virginia University, Morgantown, WV 26506.

[5]Deceased November 29, 2011.

[6]To whom correspondence may be addressed. Email: wcavenee@ucsd.edu, emmanuel@cipe.accamargo.org.br, rpasqual@salud.unm.edu, or warap@salud.unm.edu.

[7]E.D.-N., R.P., and W.A. contributed equally to this work.

This article contains supporting information online at www.pnas.org/lookup/suppl/doi:10.1073/pnas.1507882112/-/DCSupplemental.

Significance

Prostate cancer has an unpredictable natural history: While most tumors are clinically indolent, some patients display lethal phenotypes. Serum prostate-specific antigen is the most often used test in prostate cancer but screening is controversial. Treatment options are limited for metastatic disease, hence the need for early diagnosis. Prostate cancer antigen 3 (*PCA3*), a long noncoding RNA, is the most specific biomarker identified and approved as a diagnostic test. However, its inherent biological function (if any) has remained elusive. We uncovered a negative transdominant oncogenic role for *PCA3* that down-regulates an unrecognized tumor suppressor gene, *PRUNE2* (a human homolog of the *Drosophila* prune gene) thereby promoting malignant cell growth. This work defines a unique biological function for *PCA3* in prostate cancer.

PCA3 is a spliced intronic antisense lncRNA embedded within intron 6 of the corresponding sense gene *PRUNE2* (2, 7–10) (Fig. 1*A*). We hypothesized the existence of a functional role between *PCA3* and PRUNE2, and their involvement in prostate cancer progression. To study this possibility, we investigated *PRUNE2* as well as the *PCA3* intronic antisense transcripts, which we cloned from MDA-PCa-133, a patient-derived xenograft (PDX) of bone metastasis from prostate cancer (11) (Fig. 1 *A* and *B*). We next analyzed the expression of *PRUNE2* in representative panels of human tumors and nonmalignant cell lines by quantitative gene expression profiling with primers located in the *PRUNE2* exons that flank *PCA3* (Tables S1 and S2 and Fig. S1 *A* and *B*). *PRUNE2* was detectable in prostate cancer cell lines, with the highest levels in androgen-dependent (LNCaP) cells, as well as in several brain and breast lines. We also analyzed *PRUNE2* levels alongside *PCA3* lncRNA in prostate cancer cells and observed differential expression of the two genes: LNCaP cells displayed the highest levels of both *PRUNE2* and *PCA3* relative to androgen-independent (DU145 and PC3) cells (Fig. S1*C*). We confirmed the expression of native or recombinant V5-tagged PRUNE2 by immunoblot analysis, and the predicted endogenous protein (~337 kDa) was observed in LNCaP but not in PC3 cells (Fig. S1 *D* and *E*).

***PCA3* lncRNA Binds *PRUNE2* Pre-mRNA and Regulates Its Levels.** Given that *PCA3* is embedded within intron 6 of *PRUNE2*, and is transcribed in the antisense direction, we hypothesized that a double-stranded (ds)RNA forms between *PCA3* lncRNA and *PRUNE2* pre-mRNA to regulate PRUNE2 levels in prostate cancer. To evaluate this possibility, we first generated prostate cancer cell lines (LNCaP and PC3) stably transduced with ectopic *PCA3*, *PCA3*-shRNA, ectopic *PRUNE2*, *PRUNE2*-shRNA, or the corresponding controls. Levels of endogenous PRUNE2 protein, pre-mRNA and mRNA increased with *PCA3* silencing and decreased with ectopic *PCA3* expression (Fig. 1 *C* and *D* and Fig. S1 *F–H*). We confirmed these findings in prostate- and prostate cancer-derived cells, where ectopic *PCA3* expression induced down-regulation of endogenous PRUNE2 expression (Fig. S2*A*). To determine whether *PRUNE2* and *PCA3* form a dsRNA, we used co-RNA-FISH assays. *PCA3* and *PRUNE2* hybridized in the same nuclear foci (Fig. 1*E* and Fig. S2*A*). These foci were completely depleted on treatment with RNase III, which degrades only dsRNA, but not with RNase A, which degrades only single-stranded (ss)RNA (Fig. 1*E* and Fig. S2*B*), indicating the formation of dsRNA from the physical association of *PCA3* and *PRUNE2* pre-mRNA. Next, to evaluate whether binding of *PRUNE2* mRNA to *PCA3* was required for the regulation of PRUNE2 levels, we assessed the effect of *PCA3* on exogenous mature *PRUNE2* cDNA, which has no sequence complementarity to *PCA3* and therefore would be unable to form a dsRNA. Indeed, ectopic *PCA3* did not affect the exogenous expression of PRUNE2 mRNA and protein (Fig. S3*A*). To complement this finding, we also designed and expressed a *PRUNE2* construct that contains no protein-coding sequence but is still fully complementary to *PCA3* (termed intron6-*PRUNE2*) and should therefore be able to bind *PCA3* and possibly sequester it from *PRUNE2*. Consistent with this, overexpression of intron6-*PRUNE2* caused an increase in endogenous *PRUNE2* mRNA in the cytoplasm and a concomitant reduction in the nucleus (Fig. 1*F*). We confirmed a direct interaction between *PCA3* and its corresponding antisense sequence (intron6-*PRUNE2*) by using RNase-resistant assays and co-RNA-FISH in tumor cells expressing both sequences (Fig. S3 *B–E*). These data suggest that *PCA3* binding to *PRUNE2* pre-mRNA controls PRUNE2 levels.

ADARs Bind *PRUNE2/PCA3* dsRNA and Regulate PRUNE2 Levels. ADAR proteins are key regulatory enzymes for RNA editing and sequestering of noncoding RNA sequences, such as introns and untranslated mRNAs (5, 11–13), derived from the hybridization of retroinverted Alu elements (5, 13), with conversion of adenosine-to-inosine (A-to-I) RNA editing after nuclear dsRNA formation. Thus, we hypothesized that *PCA3-PRUNE2* dsRNA may be regulated by ADAR-mediated RNA editing. To test this possibility, we used quantitative RT-PCR (qRT-PCR), co-RNA-FISH, and RNA-ChIP. We found that endogenous *PCA3* and *PRUNE2* pre-mRNAs colocalize to nuclear foci associated with

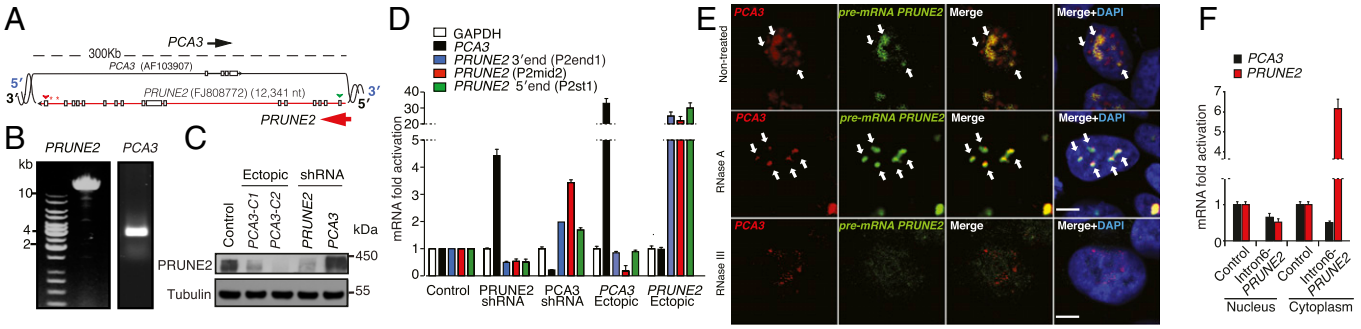

Fig. 1. *PRUNE2/PCA3* cloning, genomic structure, and colocalization. (*A*) Genomic context of intron/exon boundaries of *PCA3* and *PRUNE2* (GenBank accession no. FJ808772). Stars indicate missing or new exons; arrowheads indicate initiation (green) or stop (red) codons. Arrows indicate transcript orientation (black, *PCA3*; red, *PRUNE2*). (*B*) RT-PCR with RNA from the PDX MDA-PCa-133 used to clone/sequence *PRUNE2*. (*C*) Analysis of PRUNE2 in LNCaP cells stably expressing ectopic *PCA3*, *PCA3*-silenced, *PRUNE2*-silenced, or control. (*D*) qRT-PCR assays with primers (Table S1) amplifying *PCA3* or different regions of *PRUNE2* in LNCaP cells with silenced or ectopic *PRUNE2* and *PCA3*. (*E*) Combined RNase resistance and RNA-FISH analysis. Before hybridization, LNCaP cells were treated with RNase A or RNase III. Hybridization was performed with specific probes against *PCA3* and *PRUNE2* transcripts. Nuclei are stained with DAPI. Arrows indicate foci. Confocal images are shown (bar, 10 μm). Fig. 1*E* represents 100× magnifications (from Fig. S3*A*). (*F*) Expression effects of intron6-*PRUNE2* on nuclear and cytoplasmic *PCA3* and *PRUNE2* levels in LNCaP cells. Shown data are mean ± SD.

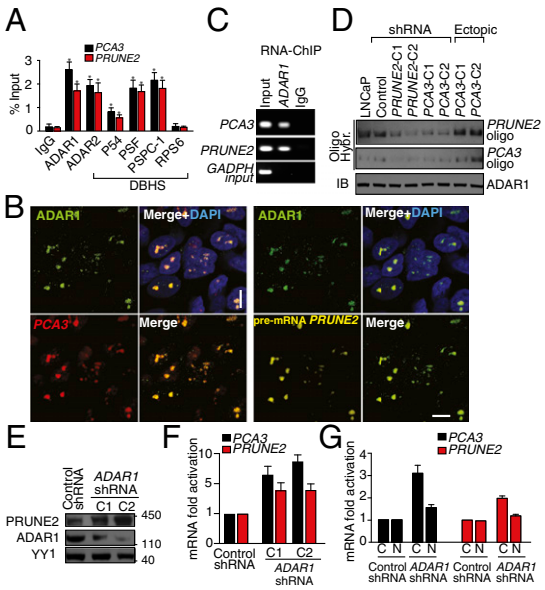

Fig. 2. *PRUNE2/PCA3* colocalization to ADAR1. (*A*) RNA-ChIP and *PCA3* and *PRUNE2* binding by qRT-PCR in LNCaP cells. (*B*) Combined RNase resistance and RNA-FISH analysis. Before hybridization, LNCaP cells were treated with RNase A. Hybridization and immunostaining were performed with specific probes and an anti-ADAR1 antibody. (*C*) *PCA3* and *PRUNE2* binding to ADAR1 by RNA-ChIP. (*D*) Hybridization with biotin-labeled oligomers (Table S1) against *PCA3* and *PRUNE2* in LNCaP cells after UV-induced RNA-protein cross-linking. Immunoblot against ADAR1 is shown. (*E* and *F*) Evaluation of *PCA3* and PRUNE2 expression in LNCaP cells stably expressing two independent lentiviral *ADAR1*-shRNAs: immunoblots against PRUNE2, ADAR1, and control protein (YY1) (*E*) and qRT-PCR (*F*) are shown. (*G*) Cytosolic (C) and nuclear (N) RNA fractionation followed by qRT-PCR; specific oligonucleotides served for amplification of nuclear pre-mRNA and cytosolic mRNA of *PCA3* and *PRUNE2*. Shown data are mean ± SD. $*P < 0.05$; $**P < 0.01$.

ADAR proteins, which were sensitive to RNase III treatment (Fig. 2 *A–C* and Fig. S4). *PRUNE2/PCA3* dsRNA and ADAR1 formed a complex only when both RNA species were coexpressed; the corresponding signals for *PRUNE2/PCA3* dsRNA decreased after *PCA3* or *PRUNE2* silencing and increased with ectopic expression of *PCA3* in a UV-induced RNA-protein cross-linking assay (Fig. 2*D*). To determine whether ADAR proteins regulate *PRUNE2* and *PCA3* levels, we silenced *ADAR1* in human tumor cells and found increased *PRUNE2* mRNA and protein levels (Fig. 2 *E–G*). We also found that ADAR-depleted prostate cancer cells have increased cytosolic *PRUNE2* and *PCA3* levels (Fig. 2 *F* and *G* and Fig. S5 *A* and *B*), revealing the importance of ADAR members in the regulation of both genes, consistent with functions of A-to-I editing in the regulation of noncoding RNA species (14). To gain functional insight into the regulation of *PRUNE2* and *PCA3*, we established sensor/reporter assays in which either *PCA3* or the *PCA3* antisense sequence (i.e., intron6-*PRUNE2*) was fused to reporters to generate *PCA3-luciferase* or *intron6-PRUNE2-GFP*. Reporter expression (by FACS and luminescence assays) showed that the coexpression of intron6-*PRUNE2-GFP* plus *PCA3* or intron6-*PRUNE2* plus *PCA3-luciferase* results in reduction of the corresponding reporter signals compared to controls (Fig. S5 *A–F*). Thus, in addition to *PCA3* regulating *PRUNE2* levels, and consistent with our earlier results, intron6-*PRUNE2* could also down-regulate *PCA3* (Fig. 1*F*). Silencing of ADAR1 or ADAR2 increased the reporter signals, confirming that these enzymes are required for a coregulatory effect on both RNAs (Fig. S5 *E–H*).

RNA Editing of *PRUNE2* and *PCA3* RNA Species. Our results thus far have indicated that ADAR proteins associate with *PRUNE2/PCA3* dsRNA and regulate *PRUNE2* and *PCA3* levels via A-to-I RNA editing. To test this possibility directly, we evaluated the presence of A-to-I editing throughout the genomic coordinates of *PCA3* and its corresponding antisense pre-mRNA intron6-*PRUNE2* by RNA capture followed by next-generation sequencing. Although RNA editing is found largely within Alu elements, we carefully filtered out repetitive elements (such as Alu sequences) to avoid erroneous alignments. We showed that A > G/T > C changes, which reflect A-to-I editing, were the most frequent substitutions. Editing sites were distributed in intronic and exonic

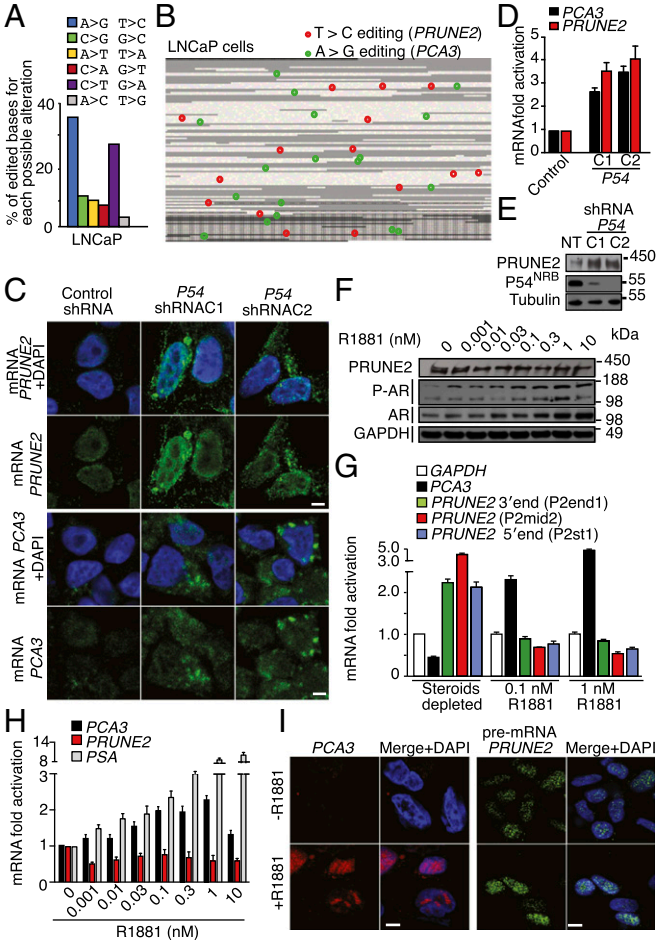

Fig. 3. Functional role of RNA editing and androgen receptor (AR) activation in PRUNE2/*PCA3* regulation. (*A* and *B*) Identification, quantification, and distribution of A > G/T > C changes (features pathognomonic of A-to-I editing in both strands of the *PRUNE2/PCA3* dsRNA) analyzed after RNA capture followed by high-throughput sequencing. Reads were aligned against hg19 of the region. Only nondbSNP variations indicated by at least three reads, and out of repetitive elements were considered. (*A*) Distribution and percentage of all possible alterations for the *PCA3* genomic coordinates in LNCaP cells are shown. (*B*) RNA editing map for LNCaP cells showing the precise location of each A > G (green) or T > C (red) sites over *PCA3* and intron6-*PRUNE2* pre-mRNA species. Each square represents one individual base from the *PCA3* locus (23,112 nt). Black borders delimit the bases of the four annotated exons (3,923 nt). Repeats (RepeatMasker) are shown in gray (*B*). (*C–E*) Evaluation of *PCA3* and *PRUNE2* levels in LNCaP cells stably expressing two independent P54^{NRB}-shRNA clones (C1 and C2) or controls (NT). Detection of *PCA3* and *PRUNE2* mRNA cytosolic levels by RNA-FISH (*C*) and by qRT-PCR (*D*) are shown. Analysis of PRUNE2 expression in LNCaP P54^{NRB}-silenced cells or negative control is shown (*E*). (*F*) Analysis of PRUNE2, AR, and phosphorylated AR (P-AR) expression in after concentration-dependent androgen stimulation with R1881. Representative PAGE 3–8% shown. (*G*) Relative mRNA expression levels of *PCA3* and *PRUNE2* transcript under R1881 stimulation. (*H*) Relative mRNA expression of *PRUNE2*, *PCA3*, and *PSA* (positive control) measured by qRT-PCR in LNCaP cells after dose-dependent R1881 stimulation. (*I*) RNA-FISH analysis for *PCA3* and pre-mRNA of *PRUNE2* in LNCaP cells under steroid-depleted conditions or after androgen stimulation.

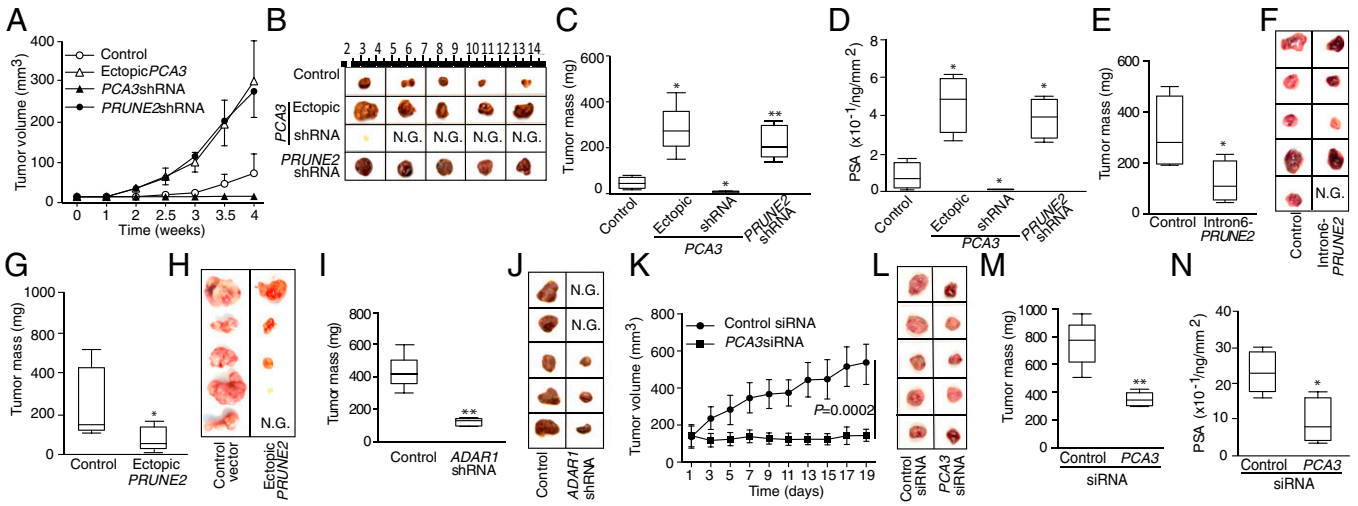

Fig. 4. PRUNE2/*PCA3* functions in tumor xenograft models of prostate cancer. (*A–D*) Male SCID mice received SC injection of 5×10^6 LNCaP cells stably expressing ectopic *PCA3*, *PCA3*-silenced, *PRUNE2*-silenced, or negative controls. Tumor growth was monitored and volume was measured (*A*). Tumors are shown after 4 wk (*B*); tumor mass (*C*) and serum PSA concentration (*D*) were determined. (*E* and *F*) Tumor growth in mice bearing LNCaP xenografts from cells stably expressing intron6-*PRUNE2* (antisense sequence to *PCA3*) or controls. Tumor growth in SCID mice bearing PC3 xenografts of cells stably expressing either ectopic PRUNE2 or negative controls (*G* and *H*) and LNCaP cells stably expressing *ADAR1*-shRNA or negative controls (*I* and *J*). (*K–N*) *PCA3* silencing in vivo by targeting SCID mice bearing LNCaP xenografts of cells stably expressing ectopic *PCA3* constructs. Two cohorts of SCID mice with size-matched tumors ($n = 10$/group) received 8 μg of stealth chemically modified *PCA3*-siRNA or negative control-siRNA per dose; treatments and controls received a series of doses ($n = 9$) through alternating intratumoral or i.p. administration every other day. Tumor volumes, measured before each administration, were plotted over time (*K*), and representative tumors at the experimental end point are shown (*L*). Tumor xenograft mass (*M*) and serum PSA concentration (*N*) were determined at the end point. In each experiment, 6–10 mice per group were treated. N.G., no growth. Mean ± SD is shown. $^*P < 0.05$, $^{**}P < 0.01$.

regions (Fig. 3 *A* and *B*), suggesting that a dsRNA hybrid is formed between pre-mRNA species of both genes, as observed in the RNA colocalization experiments. Given that the *Drosophila* behavior human splicing (DBHS) protein $P54^{NRB}$ preferentially binds to inosine-containing RNA (RNA-I) and regulates gene expression, we investigated a potential role for $P54^{NRB}$ and other DBHS proteins in regulating *PRUNE2*/*PCA3*. Both, *PCA3* and *PRUNE2* pre-mRNA species associated with $P54^{NRB}$ and the other two known mammalian family members (PSF and PSPC-1) compared with negative control RNA by RNA-ChIP (Fig. 2*A*) or combined co-RNA-FISH and immunofluorescence assays (Fig. S6). In addition, $P54^{NRB}$-silenced prostate cancer cells had increased levels of *PCA3* and *PRUNE2* mature RNA (Fig. 3 *C* and *D*) and a concomitant increase of PRUNE2 protein levels relative to controls (Fig. 3*E*). These data confirm that *PRUNE2* and *PCA3* RNAs undergo A-to-I editing and reveal a functional role for DBHS proteins in their regulation.

Function of the *PRUNE2*/*PCA3* Regulatory Axis in Prostate Cancer. Androgen dependence and resistance to androgen deprivation therapy are central to the biological and clinical features of prostate cancer. Thus, we investigated whether AR activation regulates *PCA3* and *PRUNE2* expression in androgen-dependent LNCaP cells, which had lower *PCA3* and higher *PRUNE2* levels than androgen-independent PC3 cells, when grown in steroid-depleted serum (Fig. 3 *F* and *G* and Fig. S1*C*). Androgen stimulation of LNCaP cells with a synthetic testosterone homolog (R1881) induced a concomitant increase of *PCA3* and decrease of *PRUNE2* levels (Fig. 3 *F–H*), consistent with a report that *PCA3* modulates prostate cancer through AR signaling (15). We also observed an increase in nuclear localization of *PRUNE2* and *PCA3* along with androgen-induced responses (Fig. 3*I*). Thus, *PRUNE2*/*PCA3* regulation appears to be sensitive to AR activation, a molecular hallmark of prostate cancer. To further assess the functional role(s) of the *PRUNE2*/*PCA3* regulatory axis in prostate cancer, we generated LNCaP cells (PRUNE2-expressing) or PC3 cells (PRUNE2-deficient) stably expressing lentiviral constructs to silence or ectopically express *PRUNE2* and *PCA3* (Figs. S1 *D–F* and S3*A*). *PCA3* silencing or ectopic *PRUNE2* expression decreased cell proliferation and transformation in vitro; in contrast, *PRUNE2* silencing or ectopic *PCA3* expression increased cell proliferation and transformation (Figs. S7 and S8 *A–C*). Moreover, ectopic expression of *PCA3* or antisense *PCA3* (*intron6-PRUNE2*), which downregulates *PCA3*, respectively decreased and increased endogenous, with no effect on exogenous mature *PRUNE2* expression lacking complementarity with *PCA3* (Fig. 1*C* and Figs. S2*A* and S8 *D* and *E*). Finally, we found that PRUNE2-deficient PC3 cells stably expressing ectopic *PRUNE2* had lower levels of proliferation and transformation in vitro (Fig. S8 *A* and *C*). These results are consistent with the negative regulation of *PRUNE2* by *PCA3*. We next investigated the downstream molecular mechanism(s) through which PRUNE2 suppresses tumor growth. PRUNE2 has three predicted functional domains (15): BCH, DHHA2, and PPX1 (Fig. S9*A*). BCH inhibits RhoA, a small GTPase that regulates the cytoskeleton, cell adhesion, and migration (16), whereas DHHA2 interacts with Nm23-H1, a metastasis suppressor (17). We found that endogenous PRUNE2 coimmunoprecipitates with RhoA and Nm23-H1 (Fig. S9 *B–D*). Consistent with an inhibitory role for *PRUNE2* in RhoA signaling, PRUNE2 levels increased when LNCaP cells were grown in nonadherent culture conditions (Fig. S9*E*), and the distribution of PRUNE2 was inversely correlated with focal adhesion sites in LNCaP-derived spheroids (Fig. S9 *C* and *F*). In addition, we observed alterations in tumor cell adhesion and spreading, but no effect on apoptosis (Fig. S10 *A–D*). We also noted decreased adhesion, spreading, and migration of prostate cancer cells upon PRUNE2 expression and the opposite effect on ectopic expression of *PCA3* or PRUNE2 silencing (Fig. S10 *E–J*). These results, along with the established functions of interacting proteins (16–18), suggest that PRUNE2 primarily decreases tumor growth by inhibiting cell proliferation but also affects adhesion, spreading, and migration. We subsequently extended these results to human tumor xenograft models; LNCaP prostate cancer cells stably expressing *PRUNE2*-shRNA, ectopic *PCA3*, *PCA3*-shRNA, or controls were s.c. administered into SCID mice. *PRUNE2* silencing and ectopic *PCA3* expression yielded markedly larger tumor xenografts than controls; in contrast, tumor growth was greatly diminished relative to

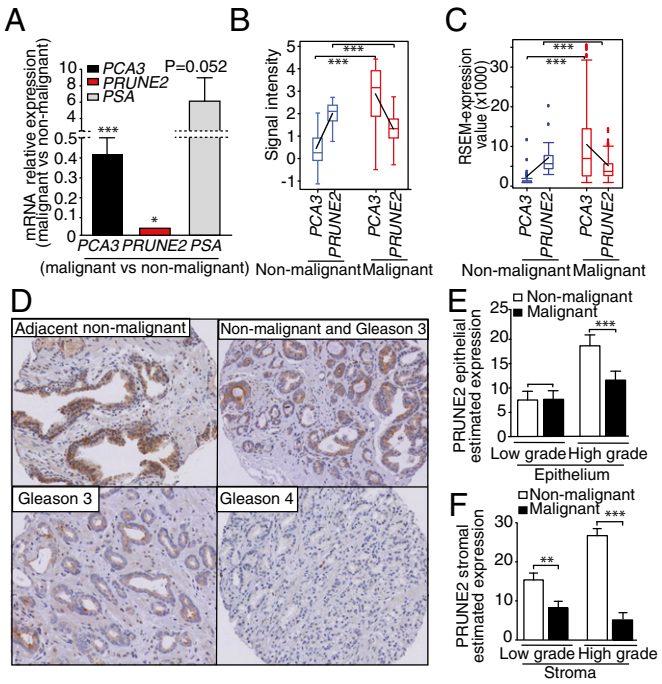

Fig. 5. PRUNE2/*PCA3* expression in prostate cancer patient samples. (*A*) Analysis of *PRUNE2* and *PCA3* mRNA levels in human prostate cancer samples ($n = 48$) vs. nonmalignant prostate tissue ($n = 9$). Malignant (M) vs. nonmalignant (NM) control is indicated. *PSA* served as a positive control for the qRT-PCR. In each case, *P* values are for M vs. NM. (*B*) *PCA3* and *PRUNE2* expression levels of cDNA microarrays from Oncomine. Blue, nonmalignant gland ($n = 29$); red, prostate tumor ($n = 115$). Box-and-whisker plots with the data are presented with the horizontal lines within boxes representing median signal intensity. Black lines depict the calculated slopes linking to average intensity values. (*C*) RSEM. Normalized RNA-Seq data from TCGA for *PCA3* and *PRUNE2* mRNA in NM (blue) or M (red) from human prostate specimens are shown. Box-and-whisker plots with the corresponding data are presented with the horizontal lines in the boxes representing the median signal intensity. Black lines depict the calculated slopes linking to average intensity values. (*D*) Human TMA of prostate cancer samples showing high-abundance of PRUNE2 in NM adjacent prostate tissue control compared with M. In each case, IHC staining (i.e., % extent of expression in cells) was analyzed. Magnification, 20×. (*E* and *F*) PRUNE2 estimated expression in the epithelium (*E*) or stromal (*F*) component of the tumor samples ($n = 145$) with low-grade ($n = 50$) and high-grade ($n = 95$) vs. NM adjacent control tissues ($n = 145$) in human prostate cancer specimens. Mean ± SD is shown. $^{**}P < 0.01$; $^{***}P < 0.001$.

controls when *PCA3* was silenced (Fig. 4 *A*–*C*). Consistently, we observed increased serum prostate-specific antigen (PSA) concentrations in SCID mice that received LNCaP cells with ectopic *PCA3* expression or *PRUNE2* silencing compared to controls (Fig. 4*D*). In vitro, and also in tumor xenograft models, expression of antisense *PCA3* (intron6-*PRUNE2*), which sequesters *PCA3*, decreased tumor growth in LNCaP but not in PC3 cells (Fig. 4 *E* and *F* and Fig. S8 *A* and *B*). Further, expression of ectopic PRUNE2 in LNCaP cells administered in SCID mice led to smaller tumors relative to controls (Fig. 4 *G* and *H*), illustrating the tumor suppressor activity of PRUNE2. Finally, silencing ADAR1, which increases PRUNE2 levels in LNCaP cells, reduced tumor cell proliferation in vitro and in vivo (Fig. 4 *I* and *J* and Fig. S11 *A*–*C*). These data show a functional role for the PRUNE2/*PCA3* regulatory axis in prostate cancer. To explore the potential of clinical application of these findings, we specifically targeted the *PCA3* sense strand with a modified siRNA (stealth RNAi-*PCA3*) serially administered to tumor-bearing mice with established prostate cancer xenografts. We observed tumor growth inhibition and serum PSA concentration reduction relative to scrambled siRNA control (Fig. 4 *K*–*N*). These results support the hypothesis that PRUNE2 expression has a functional tumor suppressive role in prostate cancer and suggest that the regulatory mechanism of PRUNE2 by *PCA3* is a molecular target for intervention.

Levels of *PCA3* and *PRUNE2* Inversely Correlate in Human Prostate Cancer Specimens. To determine the clinical relevance of our findings, we examined the expression of *PCA3* and *PRUNE2* in human prostate cancer. First, we performed qRT-PCR analysis on tumor RNA samples from prostate cancer patients ($n = 48$) and nonmalignant areas of the prostate ($n = 9$). *PRUNE2* mRNA expression was detected more often in non–tumor-containing compared with the tumor-containing areas of the prostate (Fig. 5*A*). In contrast, *PCA3* mRNA levels showed the opposite pattern, with high expression levels more frequently detected in tumors relative to nontumors, consistent with its role in the negative regulation of *PRUNE2*. To independently validate these clinical findings in silico, *PRUNE2* and *PCA3* expression levels were evaluated through Oncomine (19) in a large sample subset ($n = 144$) of primary nontreated prostate malignant tumors ($n = 115$) and nonmalignant prostate tissue ($n = 29$) (20). Although no statistically significant correlation with survival could be readily identified in this online dataset (20), a larger ongoing study is planned to fully address this question. Notably, to minimize variation, samples from prostate cancer-derived cell lines, metastatic lesions, and patients that received neoadjuvant therapy were excluded from the analysis. We next used The Cancer Genome Atlas (TCGA) as another unrelated large dataset ($n = 50$ nonmalignant control prostate samples; $n = 333$ prostate cancer samples) to validate the opposed expression between *PRUNE2* and *PCA3*. We found that low *PCA3* levels correlated with high *PRUNE2* levels in nonmalignant control prostate samples and vice

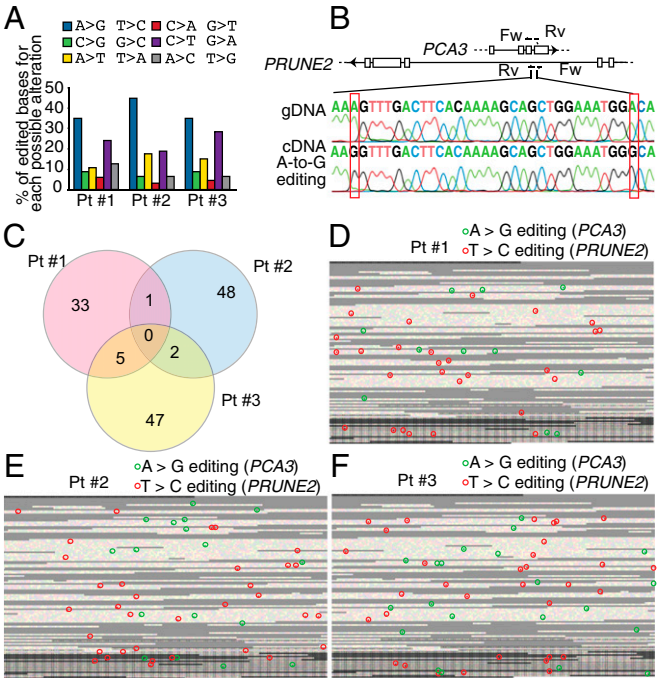

Fig. 6. RNA editing in specimens from prostate cancer patients. (*A*) All possible alterations, including putative editing sites, were determined as described for LNCaP cells and shown for each tumor sample. (*B*) A subset of editing sites suggested by large-scale sequencing was confirmed by PCR (with gDNA or cDNA as templates) followed by Sanger-sequencing. (*C*) Intersections of the putative edited sites among each independent patient sample are depicted. (*D*–*F*) Individual RNA editing maps of three prostate cancer patients are shown: Distribution of A > G (green)/T > C (red) sites over *PCA3* and intron6-*PRUNE2* pre-mRNA. Each square represents one individual base from the *PCA3* locus (23,112 nt). Black borders delimit the bases of the four annotated exons (3,923 nt). Repeats (RepeatMasker): gray.

versa in prostate cancer samples (Fig. 5 *B* and *C*). Finally, we also analyzed the protein expression pattern of PRUNE2 in a large series of clinically annotated primary prostate cancer specimens ($n = 145$), matched to adjacent histologically normal prostate tissue ($n = 145$). In each case, immunohistochemical (IHC) staining was compared between the epithelial and stromal cells within tumors to the nonmalignant epithelial and stromal cells from adjacent nonmalignant areas of the same specimen (Fig. 5 *D*–*F*). We found a higher abundance of PRUNE2 in nonmalignant vs. malignant areas. The inverse correlation between the native expression of *PRUNE2* and *PCA3* mRNA in clinical samples again supports a meaningful role for their coregulation and tumor suppression in human prostate cancer.

RNA Editing of *PCA3* and *PRUNE2* in Human Prostate Cancer Patients. We ultimately analyzed specimens obtained from index prostate cancer patients through RNA capture followed by next-generation sequencing and detected the presence of RNA editing (Fig. 6*A*), which was subsequently confirmed by classic Sanger sequencing (Fig. 6*B*) of genomic and cDNA clones from the same index patients. Bioinformatics demonstrated A > G/T > C alterations as the most frequent substitutions and data indicative of A-to-I editing in both *PCA3* and *PRUNE2* pre-mRNA strands, with no clear editing hotspots identified in human tumor samples (Fig. 6*C*). The editing maps provided for all patients show a similar distribution of alterations for both RNA strands, suggesting the interaction of the pre-mRNAs of both *PCA3* and *PRUNE2* transcripts (Fig. 6*D*).

Discussion

lncRNAs have recently emerged as central regulators of gene expression in various biological settings, but only a few have known functional roles in human prostate cancer (1, 4, 5, 21–24). Here we present extensive data that are consistent with an antisense intronic lncRNA (i.e., *PCA3*) that acts by an ADAR-mediated RNA editing mechanism to down-regulate its target gene (i.e., *PRUNE2*). In this study, we establish the functional attributes of *PCA3* as a trans-dominant negative oncogene that inactivates the unrecognized tumor suppressor gene *PRUNE2* at the RNA level through an ADAR-mediated mechanism; such a remarkable regulatory unit located in a single genetic locus appears unique to human mammalian cells. Notably, the genomic region encompassing *PRUNE2* contains several alternatively spliced isoforms (25–28), one of which is ∼3 kb shorter than the *PRUNE2* full-length sequence identified here (presumably the canonical gene) and is found in human adult nerve cells (25), with a related mouse brain-specific isoform (26); thus, other tissue-specific isoforms with different functions may perhaps exist. Tumor suppressor genes have long been shown to affect cancer growth in the classic two-hit hypothesis (29, 30). More recently, it became clear that even partial inactivation of tumor suppressors contribute critically to tumorigenesis (31), as illustrated here. In sum, we show a striking function for the clinically well-established *PCA3* marker that will lead to translational applications in human prostate cancer.

Materials and Methods

Details can be found in *SI Materials and Methods*. *PCA3* and *PRUNE2* sequence analyses were evaluated from cDNA microarray with Oncomine (19) or RNA-seq data from TCGA; expression was calculated by RNA-Seq by expectation maximization (RSEM) (32). Cell fractionation, nuclear RNA analysis, and immunoprecipitation/immunoblot were performed as previously described (13). siRNA and shRNA were custom-ordered against PCA3 or PRUNE2 (Table S1), respectively, and transfected into tumor cells (Ambion). Custom-ordered siRNAs against *PCA3* (Tables S1 and S2) were transfected into tumor cells with the NeoFX transfection reagent (Ambion). RNA FISH and confocal microscopy RNAs were performed to detect *PCA3* and *PRUNE2*. Cell culture and functional assays (cell proliferation, viability, adhesion, migration, soft agar colony formation, and tumor cell-derived spheroids) were performed. Tumor-bearing mouse models are described elsewhere (11). All animal experimentation was reviewed and approved by the Institutional Animal Care and Use Committee of the University of Texas M.D. Anderson Cancer Center (MDACC). Experiments with human samples were reviewed and approved by the Clinical Research Committee and by the institutional review board (IRB) at MDACC. All human specimens were obtained after the patients provided written informed consent under an IRB-approved experimental protocol. Total RNA samples purified from tumors from human prostate cancer patients were also obtained from the Tumor Bank at A.C. Camargo Cancer Center after IRB approval.

ACKNOWLEDGMENTS. This work was supported by National Institutes of Health Grants CA90270 (to R.P. and W.A.) and CA95616 (W.K.C.), Angel-Works, Gilson-Longenbaugh Foundation, Prostate Cancer Foundation (W.A. and R.P.), Fundação de Amparo à Pesquisa do Estado de São Paulo, and Associação Beneficente Alzira Denise Hertzog Da Silva (E.D-N.).

1. Walsh AL, Tuzova AV, Bolton EM, Lynch TH, Perry AS (2014) Long noncoding RNAs and prostate carcinogenesis: The missing 'linc'? *Trends Mol Med* 20(8):428–436.
2. Bussemakers MJG, et al. (1999) DD3: A new prostate-specific gene, highly overexpressed in prostate cancer. *Cancer Res* 59(23):5975–5979.
3. Wei JT, et al. (2014) Can urinary PCA3 supplement PSA in the early detection of prostate cancer? *J Clin Oncol* 32(36):4066–4072.
4. Esteller M (2011) Non-coding RNAs in human disease. *Nat Rev Genet* 12(12):861–874.
5. Fatica A, Bozzoni I (2014) Long non-coding RNAs: New players in cell differentiation and development. *Nat Rev Genet* 15(1):7–21.
6. Geisler S, Coller J (2013) RNA in unexpected places: Long non-coding RNA functions in diverse cellular contexts. *Nat Rev Mol Cell Biol* 14(11):699–712.
7. Machida T, et al. (2006) Increased expression of proapoptotic BMCC1, a novel gene with the BNIP2 and Cdc42GAP homology (BCH) domain, is associated with favorable prognosis in human neuroblastomas. *Oncogene* 25(13):1931–1942.
8. Clarke RA, et al. (2009) New genomic structure for prostate cancer specific gene PCA3 within BMCC1: Implications for prostate cancer detection and progression. *PLoS ONE* 4(3):e4995.
9. Lavin MF, Clarke R, Gardiner RA (2009) Differential expression of PCA3 and BMCC1 in prostate cancer. *Prostate* 69(16):1713–1714, author reply 1715.
10. Salagierski M, et al. (2010) Differential expression of PCA3 and its overlapping PRUNE2 transcript in prostate cancer. *Prostate* 70(1):70–78.
11. Lee YC, et al. (2011) BMP4 promotes prostate tumor growth in bone through osteogenesis. *Cancer Res* 71(15):5194–5203.
12. Bass BL (2002) RNA editing by adenosine deaminases that act on RNA. *Annu Rev Biochem* 71:817–846.
13. Chen L-L, DeCerbo JN, Carmichael GG (2008) Alu element-mediated gene silencing. *EMBO J* 27(12):1694–1705.
14. Mallela A, Nishikura K (2012) A-to-I editing of protein coding and noncoding RNAs. *Crit Rev Biochem Mol Biol* 47(6):493–501.
15. Ferreira LB, et al. (2012) PCA3 noncoding RNA is involved in the control of prostate-cancer cell survival and modulates androgen receptor signaling. *BMC Cancer* 12:507.
16. Soh UJ, Low BC (2008) BNIP2 extra long inhibits RhoA and cellular transformation by Lbc RhoGEF via its BCH domain. *J Cell Sci* 121(Pt 10):1739–1749.
17. Galasso A, Zollo M (2009) The Nm23-H1-h-Prune complex in cellular physiology: A 'tip of the iceberg' protein network perspective. *Mol Cell Biochem* 329(1-2):149–159.
18. Basile JR, Gavard J, Gutkind JS (2007) Plexin-B1 utilizes RhoA and Rho kinase to promote the integrin-dependent activation of Akt and ERK and endothelial cell motility. *J Biol Chem* 282(48):34888–34895.
19. Rhodes DR, et al. (2004) ONCOMINE: A cancer microarray database and integrated data-mining platform. *Neoplasia* 6(1):1–6.
20. Taylor BS, et al. (2010) Integrative genomic profiling of human prostate cancer. *Cancer Cell* 18(1):11–22.
21. Cech TR, Steitz JA (2014) The noncoding RNA revolution-trashing old rules to forge new ones. *Cell* 157(1):77–94.
22. Guttman M, et al. (2011) lincRNAs act in the circuitry controlling pluripotency and differentiation. *Nature* 477(7364):295–300.
23. Mercer TR, Dinger ME, Mattick JS (2009) Long non-coding RNAs: Insights into functions. *Nat Rev Genet* 10(3):155–159.
24. Ponting CP, Oliver PL, Reik W (2009) Evolution and functions of long noncoding RNAs. *Cell* 136(4):629–641.
25. Iwama E, et al. (2011) Cancer-related PRUNE2 protein is associated with nucleotides and is highly expressed in mature nerve tissues. *J Mol Neurosci* 44(2):103–114.
26. Arama J, et al. (2012) Bmcc1s, a novel brain-isoform of Bmcc1, affects cell morphology by regulating MAP6/STOP functions. *PLoS ONE* 7(4):e35488.
27. Harris JL, et al. (2013) BMCC1 is an AP-2 associated endosomal protein in prostate cancer cells. *PLoS ONE* 8(9):e73880.
28. Pan CQ, Low BC (2012) Functional plasticity of the BNIP-2 and Cdc42GAP Homology (BCH) domain in cell signaling and cell dynamics. *FEBS Lett* 586(17):2674–2691.
29. Knudson AG, Jr (1971) Mutation and cancer: Statistical study of retinoblastoma. *Proc Natl Acad Sci USA* 68(4):820–823.
30. Cavenee WK, et al. (1983) Expression of recessive alleles by chromosomal mechanisms in retinoblastoma. *Nature* 305(5937):779–784.
31. Berger AH, Knudson AG, Pandolfi PP (2011) A continuum model for tumour suppression. *Nature* 476(7359):163–169.
32. Li B, Dewey CN (2011) RSEM: Accurate transcript quantification from RNA-Seq data with or without a reference genome. *BMC Bioinformatics* 12:323.

Supporting Information

Salameh et al. 10.1073/pnas.1507882112

SI Materials and Methods

Reagents. Anti-BrdU (Millipore), anti−β-actin, anti−β-tubulin (ECM Biosciences), ChIP grade anti-RED1, anti−Nm23-H1, anti-RhoA (Abcam), anti-PRUNE2 (ProteinTech), anti-AKT, anti-pAKT1, anti-pERK1/2, anti-p44/42 MAP kinase, ßanti-S6RP (Cell Signaling Technology), anti-ADAR1 (Sigma or Abnova), and anti-ADAR2 (Sigma) were commercially obtained. VEGF, basic FGF (bFGF), EGF, and insulin-like growth factor (IGF) were purchased from R&D Systems. An admixture (i.e., 10 ng EGF, 10 ng bFGF, 10 ng IGF, and 20 ng VEGF) supplemented with heparin (5 U/mL) to a final concentration of 50 ng/mL served for growth factor stimulation unless otherwise specified. Methyltrienolone (R1881; Perkin-Elmer) was used for androgenic stimulation in steroid-deprived conditions as indicated. RNaseA and RNase III (Invitrogen), DNaseI-RNase free (NEB), $P54^{NRB}$, AR, pAR, and charcoal-stripped FBS (Invitrogen) were commercially obtained. Secondary antibodies were purchased from Jackson ImmunoResearch or Invitrogen.

Cell Lines and Tissue Culture. Human tumor cell lines used (HeLa, LNCaP, PC3, DU145, SF-268, SF-539, SNB-75, U-87, BT-549, Hs587T, MCF-7, NCI-ADR-RES, NCI-H322M, A549K, EKVX, NCI-H266, SK-MEL-28, UACC-257, OVCAR-8, SK-OV-3, ACHN, HEK293, TK-10, KS1767, and COLO205) were grown in RPMI containing 5% (vol/vol) FBS. Human epithelial (PrEC) and stromal (PRSC) primary prostate cells, epithelial (RWPE-1 and RWPE-2) and stromal (WPMY-1) transformed prostate cells, and prostate cancer cells (VCaP and 22Rv) were cultured in optimized medium (ATCC).

Bioinformatics and Sequence Analysis. Chromosomal locations, annotated transcripts, spliced expressed sequence tags, and sequence mapping were visualized on the Genome Browser from the University of California-Santa Cruz (https://genome.ucsc.edu), by using the latest version of the human genome assembly (hg19) available. Conserved domain analyses were performed through the Conserved Domain Database (www.ncbi.nlm.nih.gov/Structure/cdd/wrpsb.cgi), and sequence alignments were made with either ClustalW (www.ebi.ac.uk/Tools/msa/) or CLC bio (www.clcbio.com). *PCA3* and *PRUNE2* expressions were evaluated from cDNA microarray data of prostate cancer using Oncomine (1) or RNA-Seq data from the TCGA Research Network (cancergenome.nih.gov); for the latter, data were downloaded and expression values were calculated through RSEM (2) using all available samples.

Cloning and cDNA Generation. Total RNAs from tumor cell lines or xenografts were isolated through the RNeasy kit (Qiagen), the All-in-One kit (Norgen Biotek), or the TRIzol reagent (Life Technologies). Total RNA samples from human normal tissues (prostate, brain, liver, kidney, breast, lung, pancreas, spleen, and testis) were commercially obtained (Stratagene). cDNAs were synthesized by using the SuperScript III reverse transcriptase (Invitrogen or Promega) from total RNA, with N15 random pentadecamers, oligo dT primers, or specific oligonucleotides as indicated (Table S1). *PRUNE2* and *PCA3* were amplified by RT-PCR with KAPA HiFi DNA polymerase (KAPA Biosystems), cloned into pENTR directional TOPO (Invitrogen), and fully sequenced. Verified coding sequences were reamplified and subcloned into a pcDNA-DEST40 expression vector (Invitrogen). shRNA-resistant *PRUNE2* (*PRUNE2* Ω shRNA) was created by site-directed mutagenesis.

siRNA and shRNA. Custom-ordered siRNAs against *PCA3* (Table S1) were transfected into tumor cells using the NeoFX transfection reagent (Ambion). *PCA3*-silencing experiments were performed with retroviral pLKO.1 and human GIPZ vectors from the RNAi Consortium (TRC) lentiviral shRNA library (Open Biosystems) expressing specific shRNAs for human *PRUNE2* (oligonucleotide ID TRCN0000121740, referred to as *PRUNE2*-C1 and oligonucleotide ID TRCN0000144868, referred to as *PRUNE2*-C2), human *PCA3* (oligonucleotide ID V2LHS_ 24225, referred to as *PCA3*-C1; and oligonucleotide ID V2LHS_24226, referred to as *PCA3*-C2), human ADAR1 (oligonucleotide ID TRCN0000050788, referred to as *ADAR1*-C1; and oligonucleotide ID TRCN0000050790, referred to as *ADAR1*-C2 (Sigma), human GIPZ *ADAR2* (#RHS4287), and human TRIPZ lentiviral inducible shRNAmir (#RHS4740; Open Biosystems). Lentivirus particles for $P54^{NRB}$-shRNA were purchased (TRCN0000074558 referred to as $P54^{NRB}$-C1 and TRCN0000074559 referred to as $P54^{NRB}$-C2; Sigma). Stable clones were maintained under puromycin selection. Validated nontargeting siRNA (Ambion) and shRNA (Open Biosystems) sequences served as negative controls. Customized Stealth chemically modified, HPLC-purified RNAi sequences against *PCA3* or scrambled controls were purchased from Invitrogen.

Lentivirus Preparation. Lentiviral vectors (pCCLsin.PTT.PGK.EGFP.Wpre, pMDLg/pRRE, pRSV-Rev, and pMD2.VSVG) were used. Briefly, 293FT cells were transiently transfected (Lipofectamine 2000; Invitrogen) for 16 h, after which the lentiviruses were harvested 24 and 48 h later and filtered through 0.22-μm pore cellulose acetate filters. Recombinant lentiviruses were concentrated by ultracentrifugation for 2 h at 50,000 × *g*. Lentiviral vector viability was confirmed by reporter gene expression and drug selection. Cells were transfected with the FuGeneHD reagent (Roche), and transgene expression was analyzed at 24, 36, 48, or 100 h after transfection. Corresponding empty plasmids served as negative controls.

qRT-PCR and Northern Blotting. qRT-PCR analyses were performed with SYBR-green in a 7500 Fast Real-Time PCR system (Applied Biosystems). Gene expression levels were normalized against the average Ct of three standard endogenous controls (P0 large ribosomal protein, β-glucuronidase, and TATA box-binding protein), and the results were analyzed according to a standard ΔΔCt method. Data were reported as fold induction; samples were normalized onto their internal housekeeping genes followed by normalization of each sample to its control. For Northern blotting, customized LNA oligonucleotides (Exiqon) were used for *PCA3* and *PRUNE2* (Table S1). For retro-transcription, we designed specific antisense primers for *PCA3* or *PRUNE2* that allowed generation of specific cDNAs from corresponding pre-mRNA overlapped regions that enabled the generation of strand-specific cDNAs and PCR products for either *PCA3* or *PRUNE2*. Amplified products were confirmed by sequencing.

Cell Fractionation and Nuclear RNA Analysis. Nuclear/cytoplasmic RNA fractionation was performed (3). Tumor cells were grown in fibronectin-coated plates. At 70% confluence, cells were harvested, centrifuged, and rinsed with ice-cold PBS. In brief, cell pellets were resuspended by gentle pipetting in 200 μL lysis buffer A [10 mM Tris (pH 8.0), 140 mM NaCl, 1.5 mM $MgCl_2$, 0.1% octylphenoxy poly(ethyleneoxy)ethanol (IGEPAL), and 2 mM vanadyl ribonucleoside complex] and were incubated on ice for

5 min. The same lysate sample served for total RNA extraction by the TRIzol reagent (Invitrogen) and for centrifugation (1,000 × *g* for 3 min at 4 °C), as well as to isolate the cytoplasmic fraction and pellet the nuclei. Cell equivalent amounts of cytoplasmic and nuclear RNA samples were used for nuclear retention analysis. Nuclear/cytoplasmic ratios were normalized to *GAPDH, HYOU1,* or *SON* RNA controls.

RNA FISH and Confocal Microscopy. To detect *PCA3* and *PRUNE2* RNAs, cells were fixed in 3.6% (vol/vol) formaldehyde for 3 min at room temperature, followed by acetone:methanol 1:1 (vol/vol) for 5 min at −20 °C. Cells were permeabilized in PBS containing 0.39 Triton X-100 and 5 mM vanadyl ribonucleoside complex (Invitrogen) on ice for 5 min; vanadyl ribonucleoside complex (an RNase inhibitor) was omitted if the RNase enzymatic activity was to be determined. Cells were washed three times in PBS for 10 min and rinsed once in 2× saline sodium citrate (SSC) buffer before hybridization. Hybridization was carried out using labeled cy3, cy5, and 488 nm DNA-oligonucleotide probes in a moist chamber at 37 °C overnight (ON). For colocalization studies after in situ hybridization, cells were fixed for 5 min in PBS-containing 2% (vol/vol) formaldehyde. Standard immunofluorescence and imaging were performed.

Immunoprecipitation and Immunoblot Analysis. Immunoprecipitation assays were performed as previously described (3). Briefly, a total of 3×10^6 subconfluent cells were starved for 36 h in RPMI containing 0.25% BSA and 0.05% FBS. Cells were stimulated for 15 min at 37 °C with a growth factor admixture described above. After washes with ice-cold PBS containing 0.1 mM sodium orthovanadate, cells were solubilized in 1 mL lysis buffer [50 mM Tris(hydroxymethyl) aminomethane HCI (pH 7.4), 150 mM NaCl, 1% Nonidet P-40 (Nonidet P-40), 0.25% sodium deoxycholate, 1 mM EGTA, 1 mM EDTA, 2.5 mM sodium pyrophosphate, 1 mM sodium fluoride, 1 mM β-glycerophosphate, 1 mM sodium orthovanadate (Na_3VO_4) (pH 10.0), anti-protease, and anti-phosphatase mixture; (Sigma)], collected, and incubated on ice for 10 min. Cell lysates were centrifuged at 10,000 × *g* for 15 min, and supernatants were precleared for 1 h at 4 °C by incubation either with 15 μL protein A- or protein G-agarose (Roche). Precleared lysates were subsequently used for immunoprecipitation with specific antibodies as indicated. After incubation, the solution was centrifuged at 1,000 × *g* for 4 min and washed three times with 0.5 mL lysis buffer and once with ice-cold PBS containing 1 mM Na_3VO_4. Immunoprecipitates were separated by 3–8%, 4–12%, or 4% bis-Tris NuPAGE (Invitrogen) as indicated, transferred to nitrocellulose membranes, and immunoblotted with specified antibodies.

RNA–Protein Complex Immunoprecipitation. Tumor cells at 70% confluence were rinsed twice and scrapped into ice-cold PBS. Cell pellets were resuspended in immunoprecipitation buffer [50 mM Tris·HCl (pH 7.4), 150 mM NaCl, 0.05% IGEPAL, 1 mM PMSF, and proteinase inhibitor mixture (Sigma)], subjected to two rounds of gentle sonication, and centrifuged to obtain cell extracts. For RNaseA treatment, 200 μg/mL RNaseA was added to cell extracts, and the admixture was incubated at 37 °C for 30 min. For immunoprecipitation, RNaseA-treated and nontreated cell extracts were precleared with 40 μL protein-A- plus protein-G-agarose beads (Roche) and 2.5 μg mouse anti-ADAR1 antibody or irrelevant isotype control antibody at 4 °C for 2 h, followed by 40 μL protein-A- plus protein-G-agarose beads for 30 min at room temperature.

UV Cross-Linking and ChIP. Subconfluent cells cultured in complete RPMI for 24 h underwent UV-mediated cross-linking, extract preparation, and SDS/PAGE or standard immunoprecipitation. For Western blot oligo-hybridization, specific 3′-biotinylated oligonucleotides (Table S1) were used.

Cell Proliferation, Cell Viability, and Cell Death Assays. Cells were seeded in 200 μL growth medium at a density of 5,000–10,000 cells per well onto E-Plates 96 (Roche). Cell attachment and growth were monitored every 15 min for 48–72 h with real-time cell electronic sensing (RT-CES) technology (Roche). The assay system expresses impedance in arbitrary cell index (CI) units. The CI at each time point is defined as (Rn-Rb)/15; where Rn is the cell-electrode impedance of the well when it contains cells, and Rb is the background impedance of the well with the medium alone. Cell proliferation comparable data were measured 72 h later with the WST-1 cell proliferation reagent (Roche). Cell viability was evaluated by the Trypan blue-exclusion methodology. Cell death assays were performed through a standardized cell death detection ELISA kit (Roche). In brief, cells were cultured in complete RPMI medium for 24 h. After cell lysis, the cytoplasmic fraction was prediluted to 1:10 (vol/vol) with incubation buffer and tested for nucleosomes in the immunoassay substrate reaction.

Cell Adhesion and Migration Assays. Cells were seeded in 200 μL RPMI medium supplemented with 2.5% (vol/vol) FBS plus 50 ng of a growth factor admixture (described above) at a density of 5,000–10,000 cells per well onto E-Plates 96 (Roche). Cell adhesion was monitored every 15 min, during 4 h through RT-CES technology (Roche). A 24-well in colorimetric format (CytoSelect; Cell Biolabs) was used for cell migration assays. Briefly, a cell suspension (1,000 cells) was placed in the upper chamber, and RPMI medium containing 2.5% (vol/vol) FBS plus the growth factor admixture was placed in the lower chamber and incubated at 37 °C and 5% CO_2 for 4 h. Cell migration was subsequently quantified.

Cell Cycle Analysis. Cells were synchronized in RPMI containing 0.2% BSA and stimulated with 10% (vol/vol) FBS for 24 h. Proliferating cells were labeled by administration of BrdU at 10 μM for 1 h (Sigma-Aldrich). Cells were harvested by trypsinization, washed in ice-cold PBS, and fixed in 100% ethanol for 30 min on ice. DNA denaturation was achieved by incubation of fixed cells in 2 N HCl containing 0.05% Triton X-100 for 30 min at room temperature. Residual acid was neutralized with 0.1 M sodium borate (pH 8.5). Samples were incubated with an anti-BrdU monoclonal antibody, followed by cy-3–conjugated secondary antibody anti-mouse IgG (Jackson ImmunoResearch Laboratories). Total DNA content was measured with 50 μM propidium iodide (PI). Flow cytometry analysis was performed in a FACS Canto II System using the FACS Diva software (Becton-Dickinson).

Soft Agar Colony Formation Assay. Standard analysis of anchorage-independent cell growth and colony formation was performed. In brief, cells transduced with the indicated constructs were suspended at either 5×10^3 or 10^5 cells per well in 2 mL of 0.35% low-melting agarose in 35-mm culture dishes containing 0.7% agarose base. Triplicates were prepared and evaluated for each construct. Colonies were allowed to form at 37 °C under standard tissue culture conditions for 21–28 d. After incubation, staining of the formed colonies with 0.005% crystal violet (CV) enabled visual inspection, photographs, and optical density measurements after CV solubilization.

Confocal Analysis of Tumor Cell-Derived Spheroids. Tumor spheroids were prepared by growing 50–200 LNCaP cells in nonadherent 96-microwell culture dishes for 18 h in RPMI containing 10% (vol/vol) FBS. Spheroids were removed and cultured on fibronectin-coated slides in RPMI containing 2.5% (vol/vol) FBS plus a growth factor admixture (described above). Six hours

later, spheroids were fixed, immunostained with the appropriate antibody, and 3D analyzed for PRUNE2, RhoA, Nm23-H1, and β-tubulin localization.

RNA-Capture Library Preparation and Large-Scale Sequencing Analysis. RNA molecules derived from the *PRUNE2*/*PCA3* locus were captured and sequenced in large scale for a comprehensive analysis of A-to-I editing. For the library preparation, mature and immature RNA molecules derived from the *PRUNE2* locus (~300 kb) were captured by using 120 nucleotide (nt) probes designed for a 2× tiling coverage (eArray; Agilent). Captured RNAs were used as templates for the construction of libraries through the SureSelect RNA Target Enrichment for Illumina Paired-end Multiplexed Sequencing kit and protocol (Agilent). Libraries were sequenced by using a MiSeq instrument (Illumina) generating >3 million 150-nt reads per sample (i.e., ~450 million bases sequenced per sample). Reads were aligned to the human reference genome (hg19) with the Burrows-Wheeler Aligner (BWA-0.6.1). Repetitive regions from RepeatMasker were masked, and >400,000 on-target reads for each sample remained. After removing variants present in dbSNP (release 137), all discrepancies between the sample reads and hg19 (confirmed by at least three independent sequence reads) were considered and further analyzed through the CLC Genomics Workbench (version 6.0.3). A detailed analysis of putative ADAR1- and ADAR2-mediated editing (A > G/ T > C substitutions) was performed over the locus of interest, including the mapping of putative editing sites, the determination of editing frequency (i.e., putative edits per kilobase), and editing density (i.e., percentage of reads showing the alteration).

RNA-Editing Analysis by Sanger Sequencing. Nuclear or total RNA samples were isolated and subjected to three pulses of sonication (300 Hz) to produce RNA fragments of 1,000–2,000 nt, followed by DNaseI treatment. RNA samples were added to two different minilibraries of specific primers (designed to cover intronic, as well as exonic regions of *PCA3* and the corresponding intron6-*PRUNE2*), and the admixtures were heated to 99 °C for 10 min and ice-chilled for 5 min. Specific cDNAs for *PCA3* and *PRUNE2* were produced by reverse transcription with SuperScript II/III (Invitrogen) by using primers designed to bind intronic and exonic regions of *PCA3* and the corresponding intron6-*PRUNE2*. Resultant cDNAs were amplified by PCR (850-1,000 bp) and subcloned in the TOPO vector, and individual single colonies were picked and amplified. The A-to-I editing (reflected by A > G/T > C changes) frequency was estimated by Sanger sequencing of >100 individual clones containing the expected inserts. As evidence of RNA editing, we considered only non-dbSNP alterations located outside of repetitive elements (including *Alus*) and only those represented by at least three distinct reads.

Tumor-Bearing Mouse Assays. PC3 and LNCaP cell lines were established, each stably expressing ectopic *PRUNE2*, ectopic *PCA3*, control vector, *PCA3* silenced, *PRUNE2* silenced, and control-shRNA. In each case, stably expressing pool transduced cells and their corresponding controls were allowed to grow for 48 h to reach 85% confluence. Afterward, paired test and control tumor cells were counted, washed in serum-free medium, and resuspended to a final concentration of 5×10^7/mL in serum- and phenol-free basic RPMI medium. Cells were subsequently mixed in 50% volume of phenol-free Matrigel (Becton Dickinson), and cell suspensions (final volume of 200 μL) were administered s.c. in the right flanks of male 6-wk-old SCID mice (Charles River). Tumor xenograft growth was monitored serially over time. The MDA-PCa-133 patient-derived xenograft (PDX) has been reported elsewhere (4). Total RNA was obtained from an early tumor passage and used to clone *PRUNE2*. All animal experimentation was reviewed and approved by the Institutional Animal Care and Use Committee (IACUC) of the University of Texas M.D. Anderson Cancer Center (MDACC).

Tissue Microarray and Immunohistochemistry. A human tissue microarray (TMA) was constructed from prostate cancer patients (n = 145) and consisted of intermediate- or high-risk tumors (Gleason score ≥ 7, locally advanced ≥ pT2, peripheral zone tumors; n = 95) and low-risk tumors (Gleason score 6, peripheral zone tumors, previously untreated, who underwent prostatectomy; n = 50). Areas representative of all histologic tumor patterns of the Gleason grades were selected from the individual specimens. The TMA consisted of 1,500 cores, and each individual patient was represented by a set of 0.6-mm-diameter cores (median, 12; range, 18–53). For IHC analysis, images in each core of the TMA were acquired by the use of a BLISS imaging system (Bacus Laboratories). A standard percentage system was used for assessment of involvement (percentage of tumor cells exhibiting detectable staining). The extent of PRUNE2 protein expression was determined in tumor epithelium vs. adjacent stromal tissue; TMA slides were stained with an anti-PRUNE2/BMCC1 rabbit polyclonal antibody (ProteinTech Group) at a 1:70 dilution. The intensity of staining was scored as absent, low, or high. An automated stainer (DAKO) and standard 3,3-diaminobenzidine were used. Tumor samples were clinically annotated and selected from a serum and tissue bank supported by the National Cancer Institute (NCI) Specialized Program of Research Excellence (SPORE) in prostate cancer at MDACC. All human experimentation was reviewed and approved by the Clinical Research Committee (CRC) and by the institutional review board (IRB) at MDACC. All human specimens were obtained after the patients provided written informed consent under an IRB-approved experimental protocol. Total RNA samples purified from tumors from human prostate cancer patients were also obtained from the Tumor Bank at A.C. Camargo Cancer Center after its IRB approval.

Statistics. We summarized PRUNE2 expression in the samples by the use of standard descriptive statistics for continuous variables or tabulations for categorical variables. The primary analysis was based on the involvement score (extent of staining) alone, which was treated as a continuous variable. Statistical significance was determined by the appropriate tests. The nonparametric Wilcoxon–Mann–Whitney test served to assess differences in expression between high-grade, low-grade, and bone metastatic cases and stromal and epithelial compartments. The Student t test or Fisher's exact test was used in the data analysis for categorical variables as appropriate. To incorporate repeated measurements (e.g., TMA cores) from an individual patient, mixed-effects models were fitted to allow estimates of variability either within or among patients. The P values and SDs were reported in the data analysis with independently repeated experiments. All reported P values are two-sided, and $P < 0.05$ was considered statistically significant. Analyses were done with SAS for Windows (1999–2000; SAS Institute, release 8.1) and S-PLUS 2000 (1988–2000; Insightful Corporation, release 3).

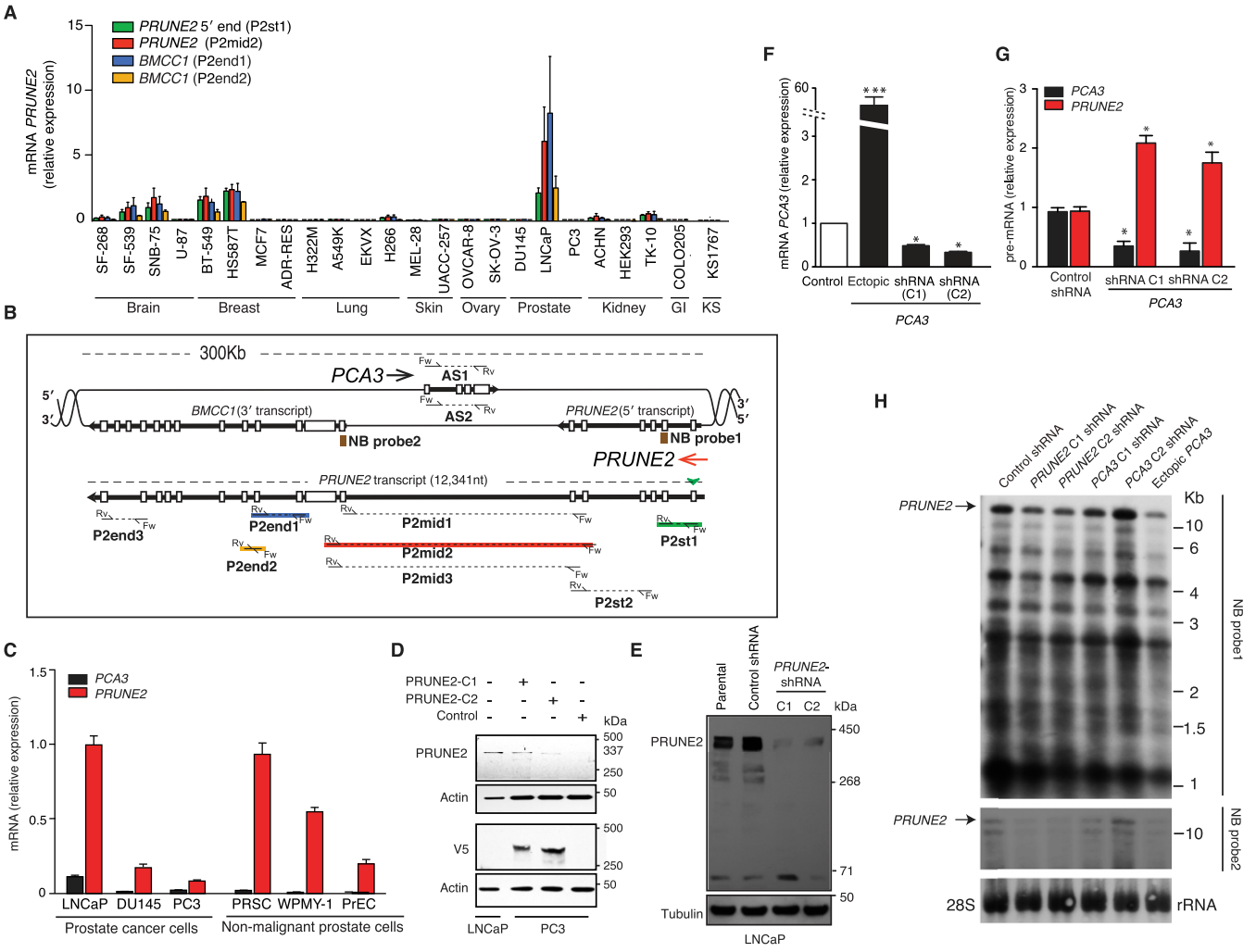

Fig. S1. Expression of *PRUNE2* and *PCA3* transcripts and related constructs in human cells. (*A*) *PRUNE2*-related mRNA levels in a representative panel of human tumor cell lines. Transcripts were amplified through qRT-PCR with a set of specific primers indicated in parentheses (Table S1). (*B*) Genomic scheme depicting intron and exon boundaries of the locus. Arrows indicate orientation of transcripts (red, *PRUNE2*; black, *PCA3*). Representation of *PRUNE2* pre-mRNA with the location of primer sets (Table S1) targeted to different regions encompassing the *PRUNE2* and *PCA3* sequences. Boxes (brown) represent Northern blot (NB) probes (NB probe 1, 5′-*PRUNE2*; NB probe 2, *PRUNE2*; Table S1) shown in *H*. (*C*) Relative mRNA expression of *PRUNE2* and *PCA3* in a panel of nonmalignant prostate-derived cells and prostate cancer-derived cells. Relative expression levels were compared against a panel of standard endogenous controls (*Materials and Methods*). Mean ± SD is shown. (*D*) Immunoblots probed with anti-PRUNE2 or anti-V5 epitope tag antibodies showing endogenous PRUNE2 expressed in prostate cancer LNCaP cells and ectopic expression of PRUNE2 in prostate cancer PC3 cells (PRUNE2-deficient). A GFP-expressing vector served as a negative control. (*E*) Immunoblotting analysis of whole cell extracts from LNCaP cells stably transduced with lentiviral shRNA constructs: two independent shRNA clones against *PRUNE2* along with a negative control (nontargeting) shRNA were used. (*F*) Changes in *PCA3* mRNA levels in prostate cancer LNCaP cells, from baseline (control shRNA), ectopic *PCA3* expression, or endogenous *PCA3*-silencing by two independent shRNA constructs (termed *PCA3*-shRNA-C1 and *PCA3*-shRNA-C2. (*G*) Relative expression of *PRUNE2* and *PCA3* pre-mRNA levels in LNCaP cells stably expressing *PCA3*-shRNA or nontargeting shRNA control. (*H*) Northern blot analysis of RNA extracted from LNCaP cells stably expressing constructs as indicated. Corresponding primers depicted in *A* and *B* are color-coded.

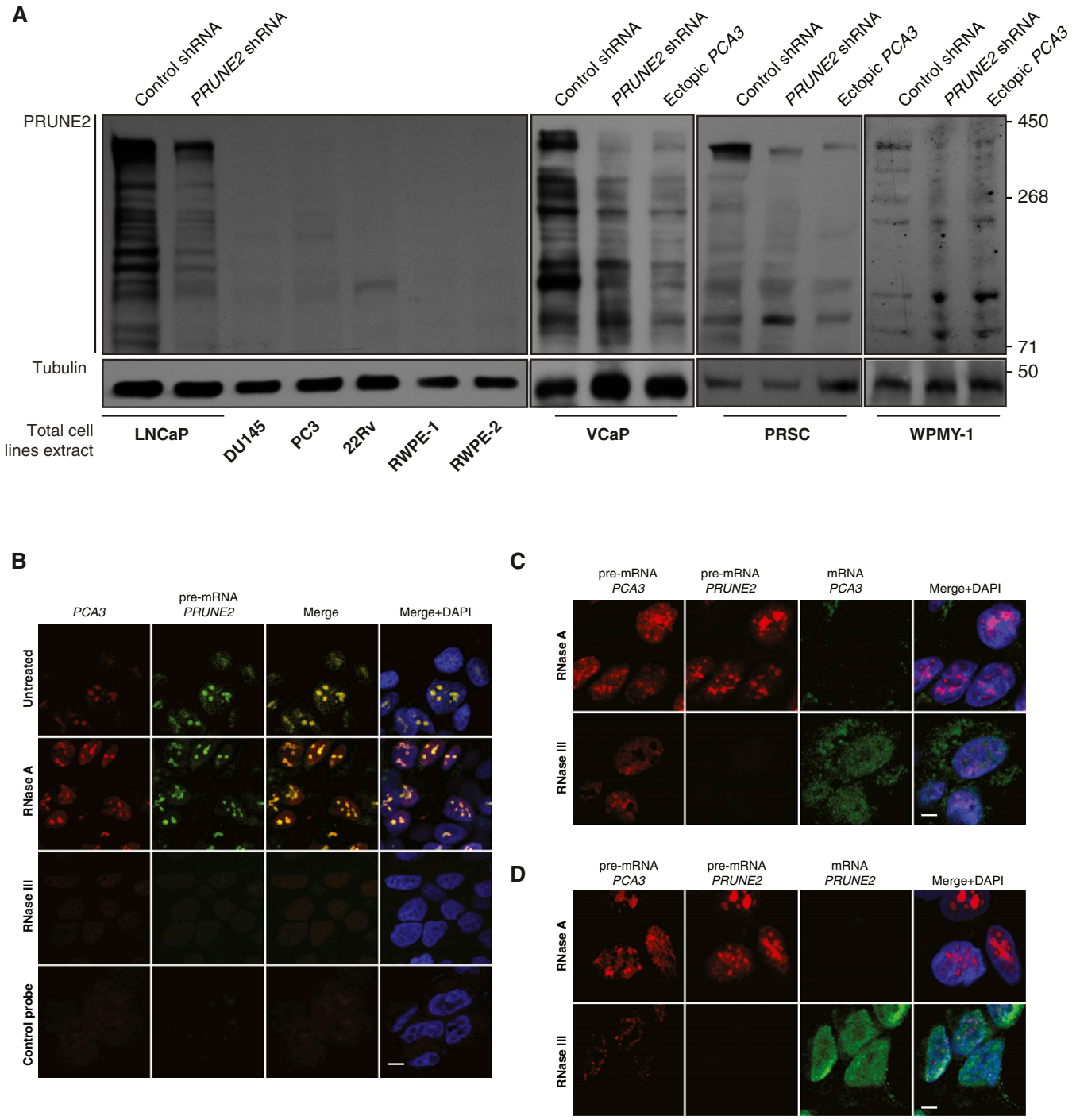

Fig. S2. PRUNE2 protein expression in human prostate- and prostate cancer-derived cells and nuclear colocalization of *PRUNE2*/*PCA3* RNA duplex. (*A*) Evaluation of *PRUNE2* protein expression by immunoblot in a representative panel ($n = 9$) of human prostate- and prostate cancer-derived cells (*Materials and Methods*) stably transduced with either *PRUNE2*-shRNA, ectopic *PCA3*, or control constructs. (*B–D*) Prostate cancer LNCaP cells were subjected to either RNase A or RNase III treatment followed by labeled oligonucleotide (Table S1) hybridization as described (*Materials and Methods*). *PCA3*-cy3 (located either in *PCA3* exon 4 for mature mRNA or in *PCA3* intron 1 for pre-mRNA; as indicated) and *PRUNE2*-cy5 (located in *PRUNE2* intron 6) oligomers were used. Pre-mRNA of *PRUNE2* (green) and mRNA of *PCA3* (red) are shown. Yellow color (merge panels) indicates *PCA3 and PRUNE2* colocalization within the nucleus (DAPI, shown in blue). Labeled oligonucleotide-cy3 and -cy5 GFP probes served as negative controls (*B*). Ribonuclease digestion controls of the pre-mRNA (red) or mRNA (green) for *PCA3* and *PRUNE2* are shown (*C* and *D*).

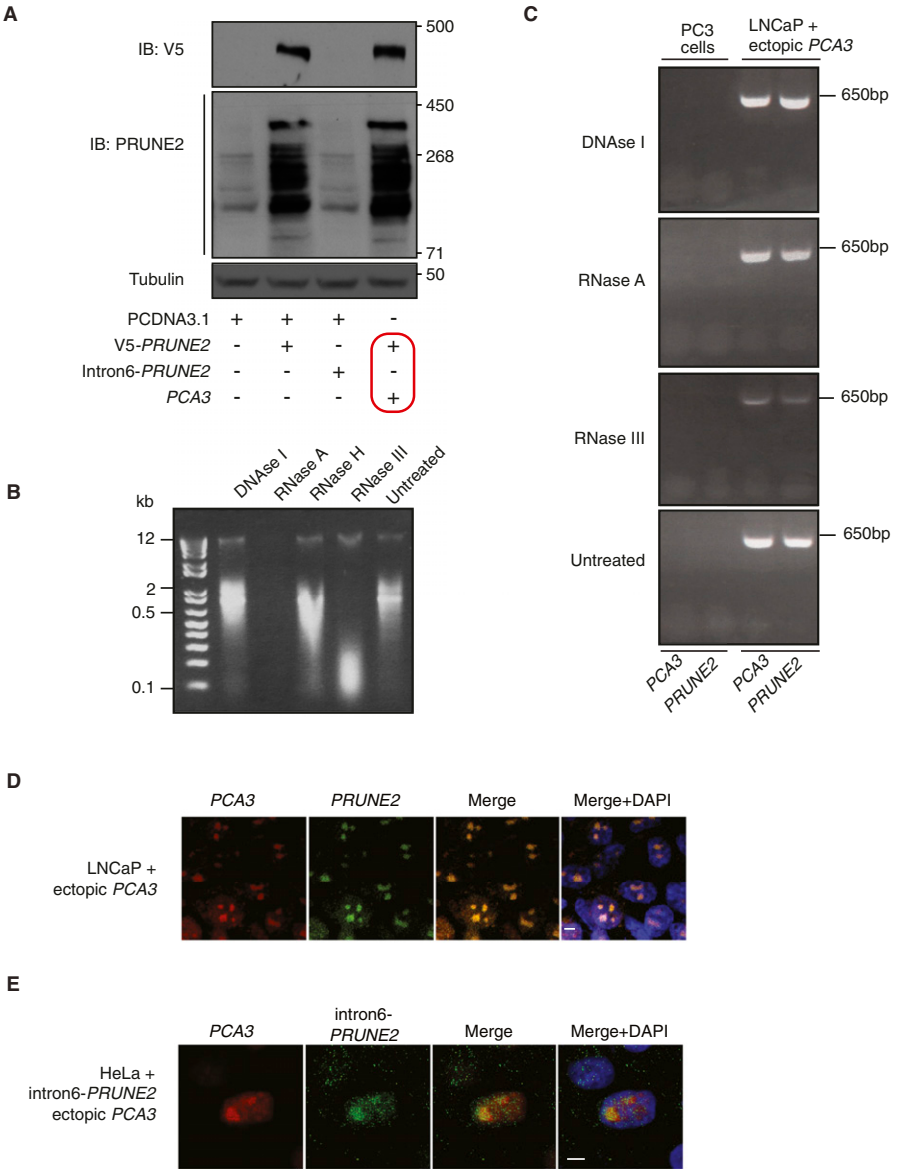

Fig. S3. Effects of *PCA3* expression on PRUNE2 coding sequence and nuclear colocalization of *PRUNE2* pre-mRNA and *PCA3*. (*A*) Analysis of combinatorial transfections in human prostate cancer PC3 cells (PRUNE2-deficient). Empty vector, *V5-PRUNE2*, intron6-*PRUNE2,* and ectopic *PCA3* were used as indicated. Immunoblots with either a V5-tag antibody or an anti-PRUNE2 antibody demonstrate that *PCA3* levels have no detectable effect on exogenous PRUNE2 expression compared to controls (outlined in red). (*B* and *C*) LNCaP cells stably overexpressing *PCA3*. RNase-resistance assay on nuclear RNA (*B*) followed by RT-PCR by using specific oligonucleotides for *PCA3* and *PRUNE2* pre-mRNA (Table S1). RNA from PC3 cells was used as negative control (*C*). (*D*) Cells were subjected to co-RNA-FISH using labeled oligonucleotides for *PCA3* (located in exon 4; red) and *PRUNE2*, in red (located in intron 6; green). (*E*) HeLa cells stably coexpressing ectopic *PCA3* and intron6-*PRUNE2* RNA were subjected to co-RNA-FISH using labeled oligonucleotides for *PCA3* (located in exon 4, red) and *PRUNE2* (located in intron 6, green). (*D* and *E*) Yellow color (merge panels) indicates PCA3 and PRUNE2 colocalization within the nucleolus (DAPI, shown in blue). Representative images are shown. (Scale bars, 10 μm.)

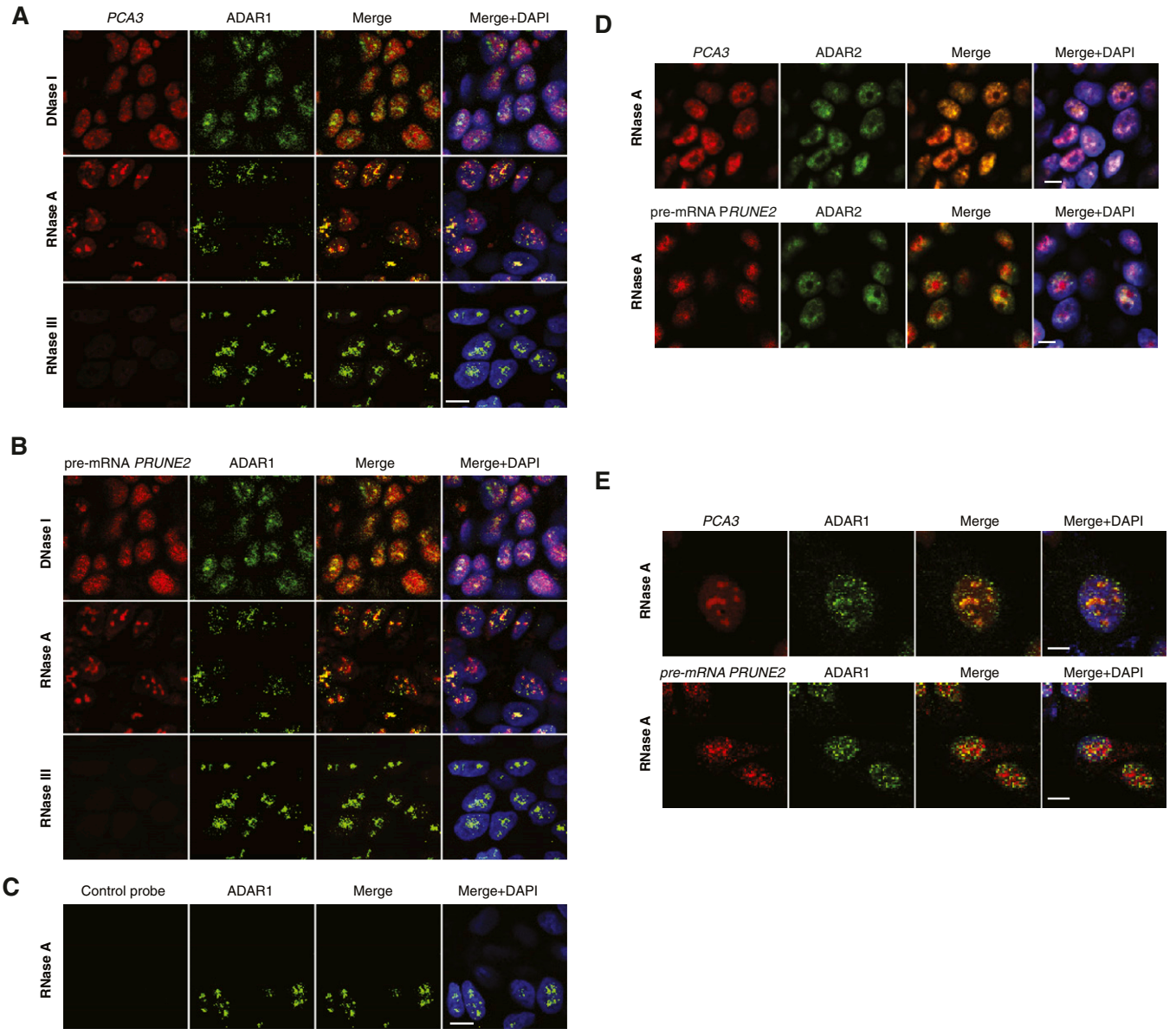

Fig. S4. Nuclear colocalization of *PRUNE2*/*PCA3* RNA duplex with ADAR1/2. (*A*–*D*) LNCaP cells were subjected to either DNase or RNase treatment as indicated, followed by oligonucleotide hybridization. Combined RNA-FISH and immunofluorescence with an anti-ADAR1 (*A*–*C*) or anti-ADAR2 (*D*) antibodies. Labeled oligonucleotides *PCA3*-cy3 (located in exon 4) and *PRUNE2*-cy5 (located in intron 6) were used. *PCA3* and *PRUNE2* (red) and ADAR1or ADAR2 (green) are shown. Yellow color (merge panels) indicates either *PCA3* and ADAR1 or ADAR2 colocalization or *PRUNE2* and ADAR1 or ADAR2 colocalization within the nucleolus (DAPI, shown in blue). Labeled oligonucleotide-cy3 and -cy5 GFP probes served as negative controls (*C*). (*E*) HeLa cells stably coexpressing *PCA3* and intron6-*PRUNE2* RNA were subjected to RNase A treatment followed by oligonucleotide hybridization. Combined RNA-FISH and immunofluorescence with an anti-ADAR1 antibody. Labeled oligonucleotides *PCA3* (located in exon 4) and *PRUNE2* (located in *PRUNE2* intron 6) were used. *PCA3* and *PRUNE2* (red) and ADAR1 (green) are shown. Yellow color (merge panels) indicates either *PCA3* and ADAR1 colocalization or *PRUNE2* and ADAR1 colocalization within the nucleolus (DAPI, shown in blue). Representative images are shown. (Scale bars, 10 μm.)

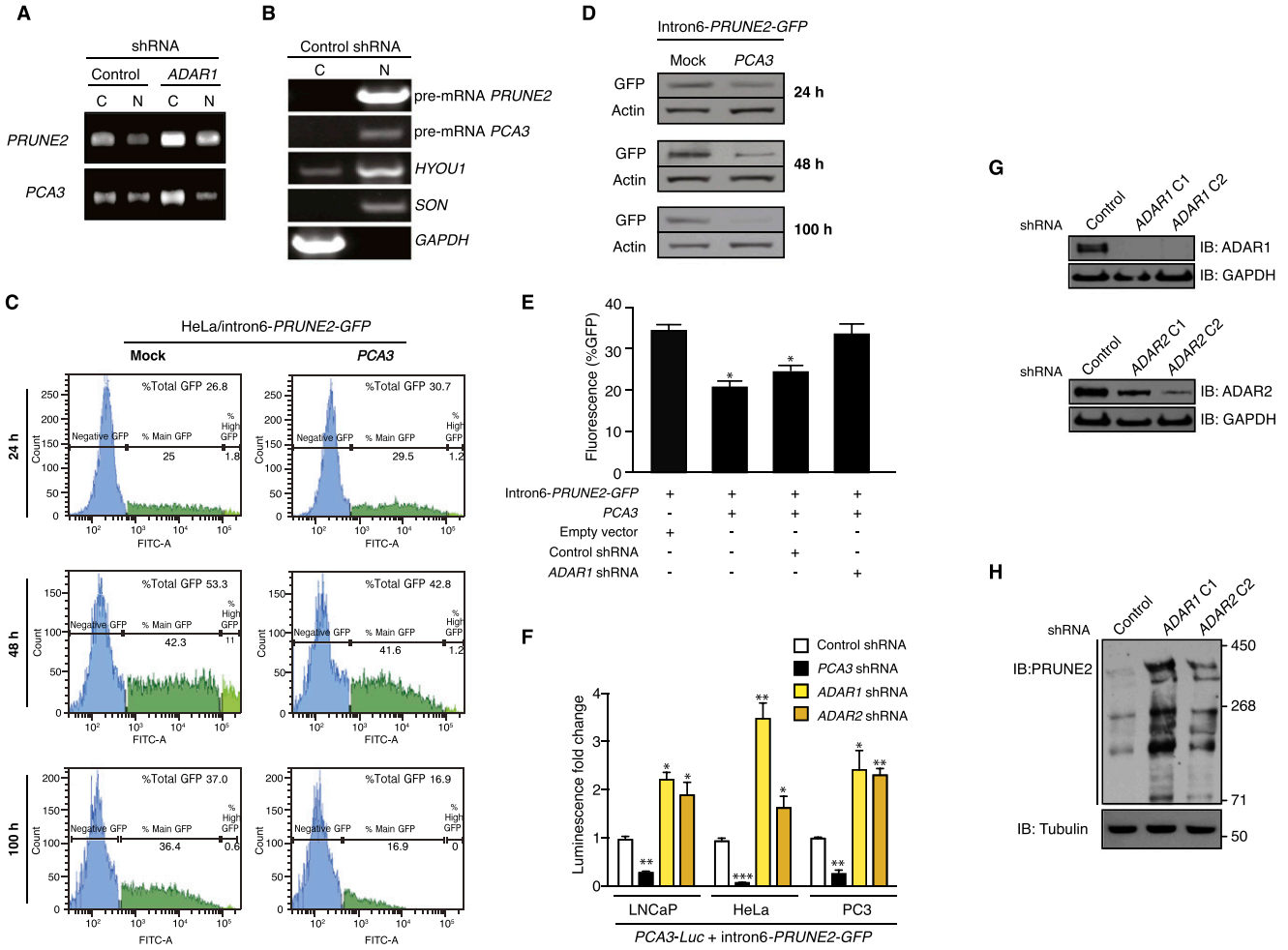

Fig. S5. Analysis *PRUNE2* and *PCA3* regulation through ADAR-mediated mechanisms. (*A*) RT-qPCR on fractionated RNA from cytosol (C) or nucleus (N) from LNCaP cells stably expressing *ADAR1*-shRNA or negative control constructs. (*B*) Quality control of cytosolic and nuclear RNA-fractionation by agarose gel electrophoresis after RT-PCR amplification. *PRUNE2* and *PCA3* pre-mRNA species are detected mostly in the nucleus as well as the controls *HYOU1* and *SON* (control nuclear mRNAs); in contrast, *GAPDH* mRNA (control cytosolic mRNA) is detected mostly in the cytosol. (*C–E*) HeLa cells stably expressing intron6-*PRUNE2-GFP* were transduced with either *PCA3* or control constructs. Cells were analyzed for reporter GFP expression by FACS (*C*) and by immunoblotting with anti-GFP antibodies (*D*) after 24, 48, and 100 h. HeLa cells stably expressing intron6-*PRUNE2-GFP, PCA3*, *ADAR1*-shRNA, nontargeting shRNA control, or negative control (empty) lentivirus were analyzed after 48 h for the reporter GFP expression (*E*). (*F*) Human tumor cell lines stably coexpressing *PCA3*-luciferase (Luc) were transduced with intron6-*PRUNE2-GFP* or negative control expression vector. Tumor cells were lysed and luciferase activity was measured at 36 h after transduction. **P* < 0.05, ***P* < 0.01, ****P* < 0.001. (*G* and *H*) Evaluation of PRUNE2 levels in LNCaP cells stably expressing ADAR1- or ADAR2-shRNA, and control lentivirus. Quality control of two individual ADAR1- and ADAR2-shRNA constructs (*G*). Whole cell extracts from LNCaP cells expressing ADAR1- and ADAR2-shRNA constructs were probed with antibodies against PRUNE2 and tubulin (*H*).

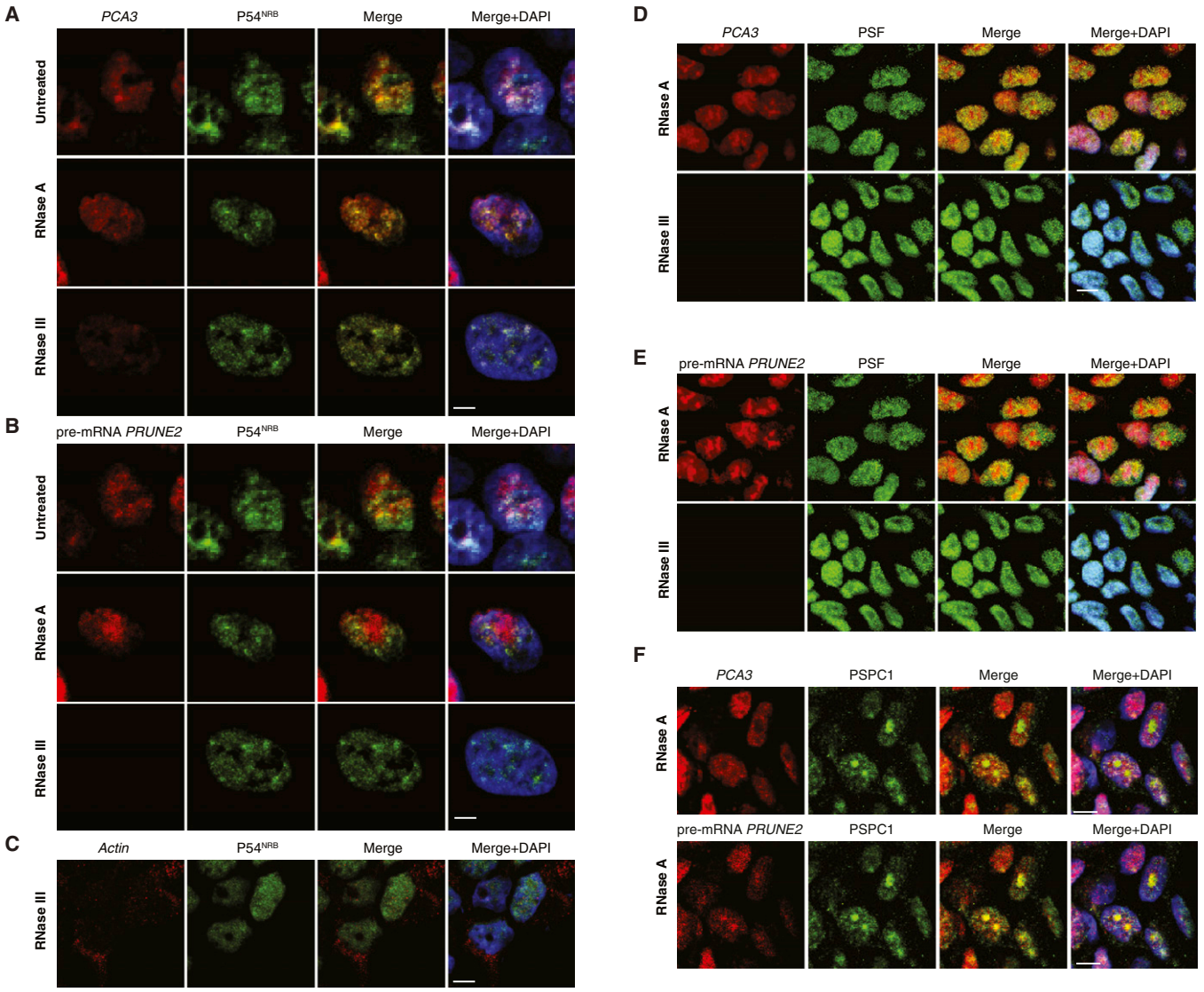

Fig. S6. Colocalization of *PRUNE2*/*PCA3* with P54^{NRB}. LNCaP cells were subjected to RNase pretreatment as indicated followed by oligonucleotide hybridization and immunofluorescence as described (*Materials and Methods*). (*A*–*C*) Detection of *PCA3*-cy3 (located in exon 4, red) and *PRUNE2*-cy5 (located in intron 6, green) by RNA-FISH and immunofluorescence with an anti-P54^{NRB} antibody. Yellow color (merge panels) indicates *PCA3* and pre-mRNA *PRUNE2* colocalization with P54^{NRB}; labeled oligonucleotide-cy3 against *Actin* mRNA (red) served as a negative control. (*D* and *E*) Combined RNA-FISH and immunofluorescence with an anti-PSF antibody. Labeled oligonucleotides *PCA3*-cy3 and *PRUNE2*-cy5 (located in intron 6) were used. *PCA3* and pre-mRNA of *PRUNE2* (red) and PSF (green) are shown. Either *PCA3* and PSF or *PRUNE2* and PSF colocalize (yellow) within the nucleus (DAPI, blue). (*F*) RNA-FISH and combined immunofluorescence with an anti–PSPC-1 antibody. A labeled *PCA3* oligonucleotide (located in exon 4) and a *PRUNE2* oligonucleotide (located in intron 6), both shown in red, and an anti–PSPC-1 antibody (shown in green) were used. Yellow color (merge panels) indicates either *PCA3* and PSPC-1 colocalization or *PRUNE2* and PSPC-1 colocalization within the nucleus (DAPI, shown in blue). (Scale bars, 10 μm.) Representative images are shown.

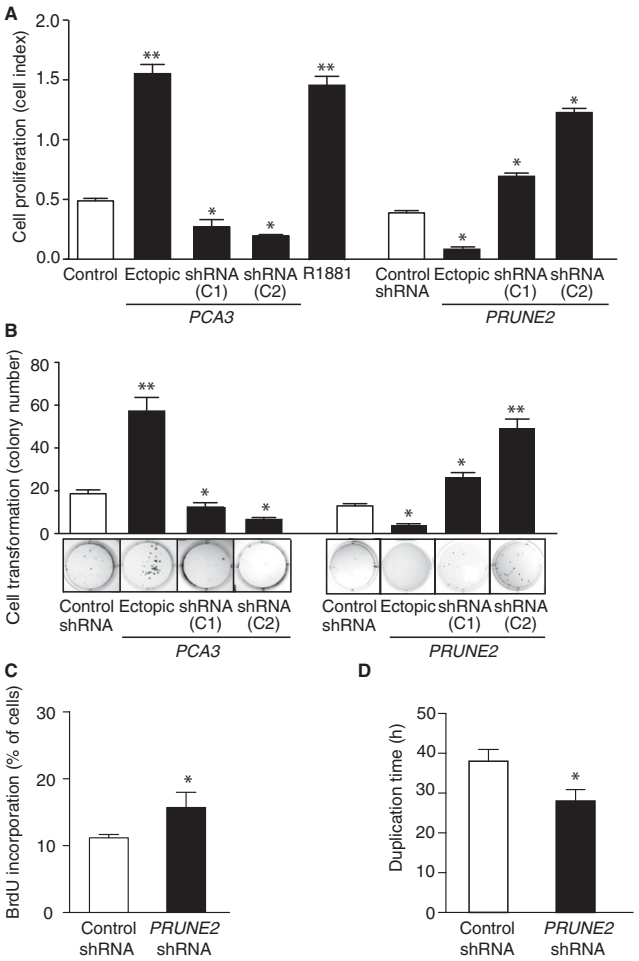

Fig. S7. Function of PRUNE2/*PCA3* in prostate cancer cells. (*A*) LNCaP cell proliferation in vitro after alteration of *PCA3* and *PRUNE2* levels or treatment with the androgen analog R1881. (*B*) Colony formation assay in soft agar medium of LNCaP cells transduced with ectopic *PCA3* or PRUNE2, *PCA3*- or *PRUNE2*-shRNAs, or controls as indicated. In each experiment, mean ± SD is shown. $*P < 0.05$; $**P < 0.01$. (*C*) Cell cycle analysis by BrdU incorporation. (*D*) Cell-doubling time.

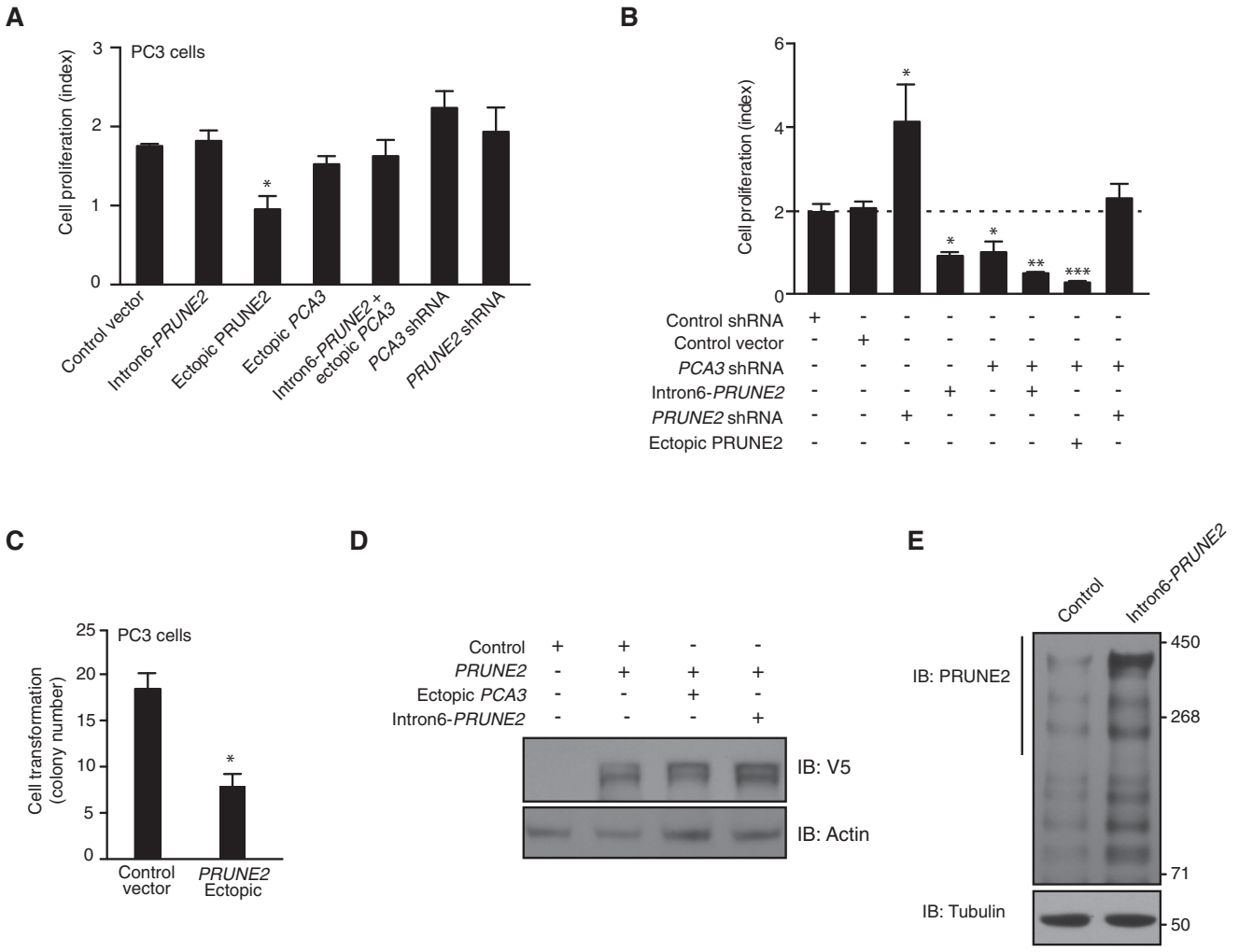

Fig. S8. Epistasis analysis of the functional interplay between PRUNE2 and *PCA3* in human prostate cancer cells. (*A*) Tumor cell growth analysis in PC3 cells stably expressing intron6-*PRUNE2*, ectopic *PRUNE2*, ectopic *PCA3*, intron6-*PRUNE2* plus ectopic *PCA3*, *PCA3*-shRNA, *PRUNE2*-shRNA, or control shRNA constructs. (*B*) Tumor cell growth analysis in LNCaP cells stably expressing *PCA3*-shRNA, *PRUNE2*-shRNA, intron6-*PRUNE2*, *V5-PRUNE2*, or control constructs. (*C*) Anchorage-independent cell colony growth in soft agar medium of PC3 cells stably expressing *V5-PRUNE2* or control vector. In each experiment, mean ± SD is shown. $*P < 0.05$, $**P < 0.01$, $***P < 0.001$. (*D*) Immunoblots of extracts from LNCaP cells stably expressing *PRUNE2*-shRNA, *PCA3*-shRNA, ectopic *PCA3*, intron6-*PRUNE2*, or control shRNA constructs. (*E*) Immunoblots of whole extracts from LNCaP cells stably transduced with *V5-PRUNE2*, ectopic *PCA3*, intron6-*PRUNE2*, or control shRNA constructs. Antibodies against V5-tag or actin were used.

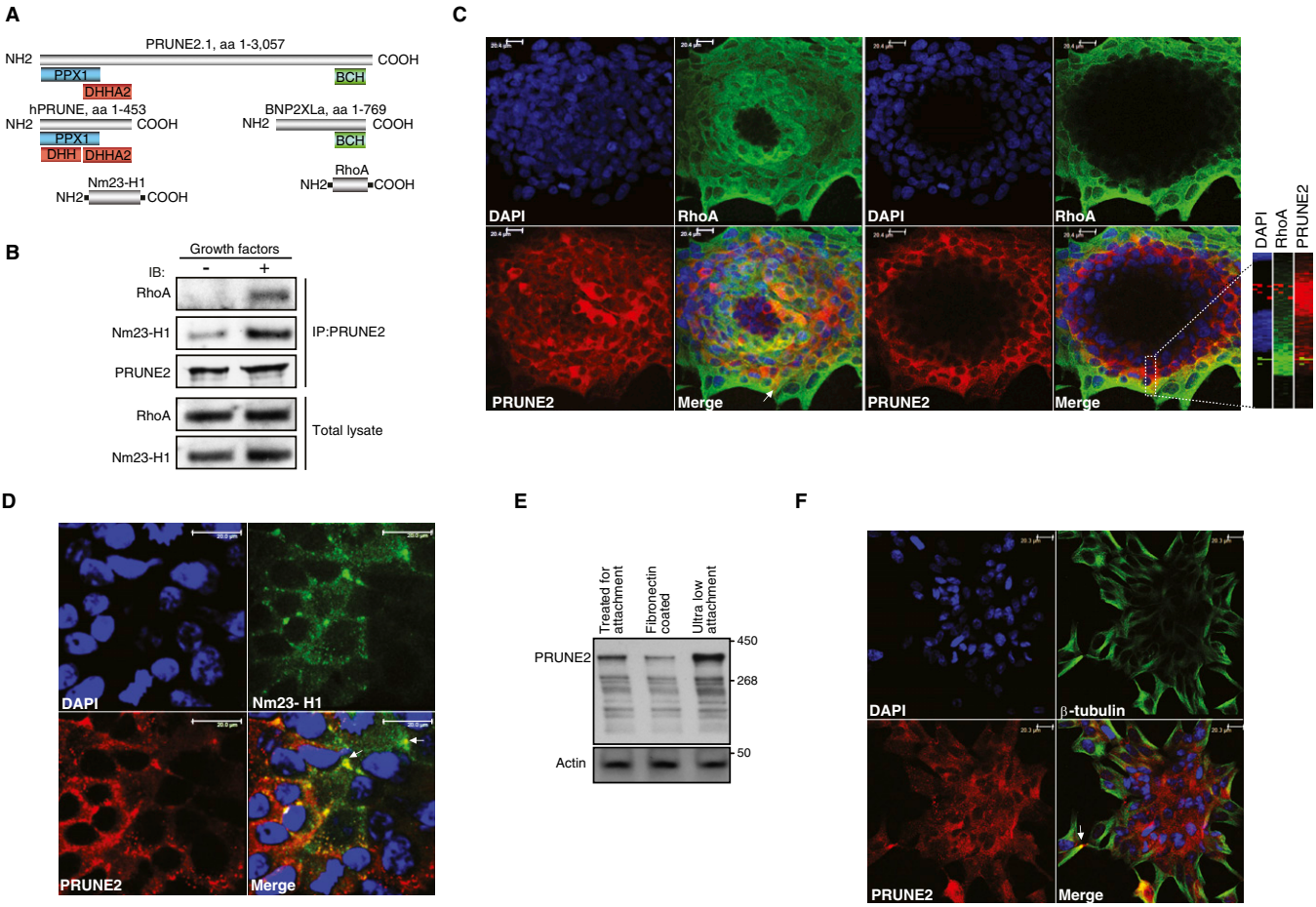

Fig. S9. PRUNE2 domains, interactions, and colocalization with RhoA and Nm23-H1. (*A*) Predicted protein domains of PRUNE2 and putative interaction sites with RhoA and Nm23-H1. Conserved domains are indicated in blue (PPX1), red (DHH and DHHA2), and green (BCH), and protein sequences are indicated in gray. (*B*) PRUNE2 coimmunoprecipitation with RhoA and Nm23-H1. Starved LNCaP cell lysates were obtained after 10-min stimulation with a growth factor admixture (GF+; *Materials and Methods*) or BSA (GF–). Immunoprecipitation was performed with an anti-PRUNE2 antibody. Both RhoA and Nm23-H1 co-precipitated with PRUNE2 on growth factor stimulation. Total cell extracts before immunoprecipitation served as loading controls. (*C* and *D*) Immunostaining and confocal microscopy analysis of the entire LNCaP-derived spheroids were reconstructed by merging the full Z-section series. Colocalization of PRUNE2 (red) with RhoA (*C*); Nm23-H1 (*D*) is shown in green. DAPI, blue. Arrows indicate protein colocalization. (*E*) Immunoblots probed for PRUNE2 in LNCaP cell lysates grown in either nonadherent or adherent conditions as indicated. (*F*) Immunostaining and confocal microscopy analysis of the entire LNCaP-derived spheroids were reconstructed by merging the full Z-section series. Colocalization of PRUNE2 (red) and tubulin (green). DAPI, blue. Arrows indicate proteins colocalization.

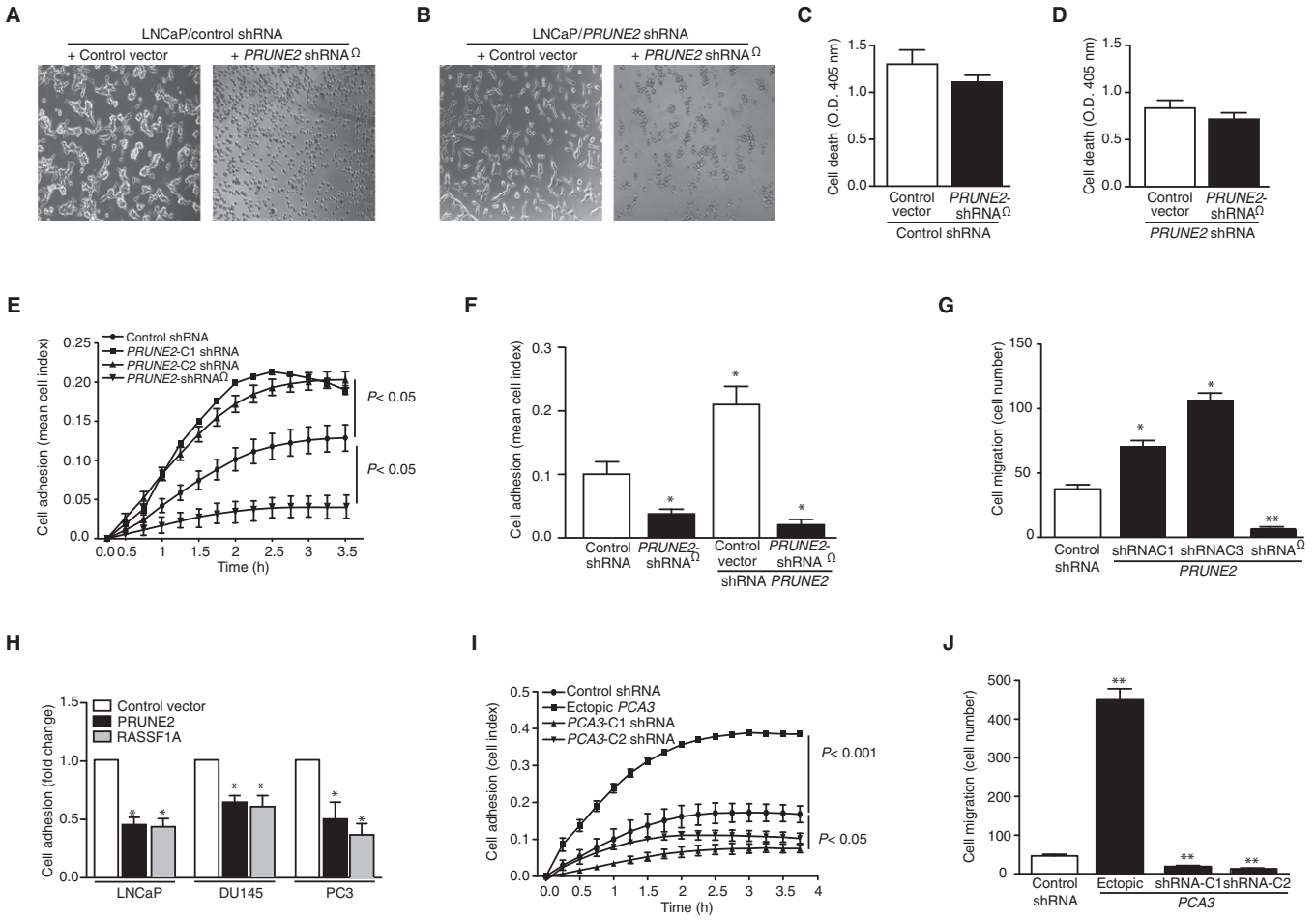

Fig. S10. Biological function of PRUNE2 in prostate cancer cells. (*A–D*) *PRUNE2* complementation assay in LNCaP cells stably expressing either control shRNA (*A*) or *PRUNE2*-shRNA (*B*) were transduced with an shRNA-resistant *PRUNE2* (PRUNE2-shRNA) construct. In both cases, PRUNE2-shRNA expression resulted in a decrease in LNCaP cell adhesion and spreading. LNCaP cells stably expressing either control shRNA (*C*) or PRUNE2 shRNA (*D*) were transduced with PRUNE2-shRNA. In both cases, ectopic expression of PRUNE2-RNA did not result in significant changes in cell death. (*E–J*) Effects of PRUNE2 overexpression on prostate cancer cell adhesion and migration. (*E–G*) LNCaP cells stably expressing *PRUNE2*-shRNA, control shRNA, or two independent *PRUNE2*-shRNA constructs were evaluated for their capacity to adhere (*E* and *F*) and migrate (*G*) in the presence of RPMI containing 2.5% (vol/vol) FBS plus a growth factor admixture. (*H*) LNCaP, DU145, and PC3 prostate cancer cells were transfected with PRUNE2, an unrelated tumor suppressor gene *RASSF1A* (as a positive control), or vector alone as a negative control and analyzed for cell adhesion. (*I* and *J*) Effect of *PCA3* overexpression on cell adhesion in LNCaP cells. Cells stably expressing *PCA3*, control shRNA, or two independent *PCA3*-shRNA constructs per gene were evaluated for their capacity to adhere (*I*) and migrate (*J*) in the presence of RPMI containing 2.5% (vol/vol) FBS plus a growth factor admixture.

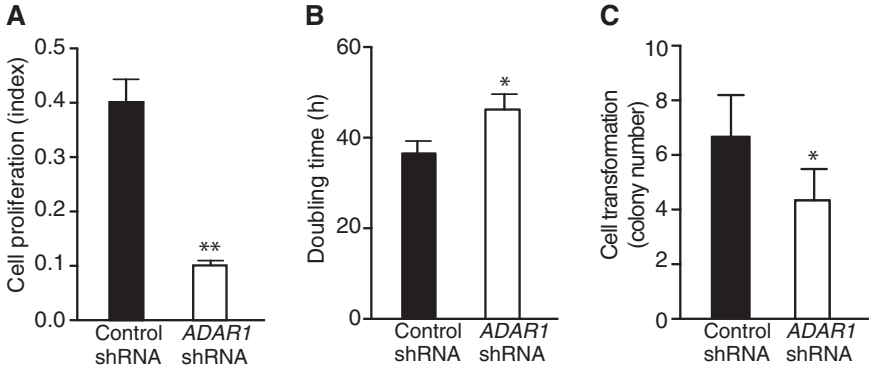

Fig. S11. Effects of *ADAR1*-silencing in prostate cancer cells. (*A–C*) Cell growth of LNCaP cells stably expressing *ADAR1*-shRNA or control shRNA. Cell proliferation (*A*), cell doubling time (*B*), and anchorage-independent colony formation in soft agar (*C*) are shown. In each experiment, mean ± SD is shown. **P* < 0.05, ***P* < 0.01.

Table S1. Oligonucleotide and probe sequences

Oligonucleotide ID	Sequence
PRUNE2 amplification	
P2.rv	5′ CCAAAACGAAGTCTAACAGACA 3′
P2.fw	5′ ACCCCGCTCGTCTTCCTT 3′
PRUNE2- C1/C2 coding sequences subcloning	
P2-1enter.fw	5′ CACCATGGAAGAATTTTTGCAACG 3′
P2-1enter.rv	5′ AGGCTTTTCTTTCAGCTTCAAGTC 3′
P2-2enter.fw	5′ CACCATGGAATCAGAGAAGATCTCAG 3′
P2-2enter.rv	5′ GAGAAGGTTACCTGAATCTCCTCC 3′
Primers for RNA CHIP	
PRUNE2 118540.fw	5′ TTTACGTTCTGGGATACATGTGC 3′
PRUNE2 121974.rv	5′ AGATCCCTGGGAGAAATGCCCGGCC 3′
PCA3 ex3.fw	5′ AAGAAAGGCTGCTGACTTTACCATCTGAGGC 3′
PCA3 ex4.rv	5′ GATCTTGAGATGCTTCCCAGCCTGTTCACAG 3′
Primers for oligo hybridization (5′ biotinylated)	
PCA3 ex4.rv	5′ GATCTTGAGATGCTTCCCAGCCTGTTCACAG 3′
PRUNE2.rv	5′ CTGTGAACAGGCTGGGAAGCATCTCAAGATC 3′
Tubulin.rv	5′ ATGCGCGAGATCGTGCACATCCAGGCGGGCCA 3′
5′-*PRUNE2*	
P2st1.fw	5′ CCACGACATGGAAGAATTTTTG 3′
P2st1.rv	5′ GCGTTTGCTTCGATTCAGTTT 3′
P2st2.fw	5′ TCTCCATCTGACAGCTCCTTTA 3′
P2st2.rv	5′ CTCATCACCGAGCAACTGGCT 3′
PRUNE2	
P2mid.fw	5′ GGAGACCCAGTTCAGTGCTC 3′
P2mid.rv	5′ TGTAAATGCTTTCAAGTCACTGGT 3′
2mid2.fw	5′ TCAGACGGTGAAATAAAAGTG 3′
P2mid2.rv	5′ AGGATCTCATCACAGCCAC 3′
P2mid3.fw	5′ AATCGAAGCAAACGCTTGGAG 3′
P2mid3.rv	5′ TGTAAATGCTTTCAAGTCACTG 3′
PRUNE2_BMCC1	
P2end1.fw	5′ CGTTTATTTGCCGGTAGGAG 3′
P2end1.rv	5′ GCTCAGGCTCTTTGGTAGGA 3′
P2end2.fw	5′ GGGAAATGCTTTCACCACAG 3′
P2end2.rv	5′ CTCTTCAAAGGGGATGTCCA 3′
P2end3.fw	5′ TCAATAGCTTATCAGAACTCAGTGG 3′
P2end3.rv	5′ TCAACAGAACCATGAACCAGA 3′
PCA3	
AS1.fw	5′ AGAAGCTGGCATCAGAAA 3′
AS1.rv	5′ CTGGAAATGTGCAAAAACAT 3′
AS2.fw	5′ TGGGAAGGACCTGATGATACA 3′
AS2.rv	5′ CCCAGGGATCTCTGTGCTT 3′
PSA AS.fw	5′ AGCATTGAACCAGAGGAGTTCT 3′
PSA AS.rv	5′ CCCGAGCAGGTGCTTTTG 3′
GAPDH AS.fw	5′ GAAGGTGAAGGTCGGAGTC 3′
GAPDH AS.rv	5′ TCAGAAGATGGTGATGGGATTTC 3′
B2M.fw	5′ AGCAGAGAATGGAAAGTCAAA 3′
B2M.rv	5′ TGCTGCTTACATGTCTCG 3′
HPRT.fw	5′ CTCAACTTTAACTGGAAAGAATGTC 3′
HPRT.rv	5′ TCCTTTTCACCAGCAAGCT 3′
Probes for FISH RNA	
CY3-PCA3 Probe-A	5′ AGTTTAGGCAGCAGGGCCAGAATCCTGACCCTCTGCCCCGTGGTTATCTCC 3′
CY3-PCA3 Probe-B	5′ CCCTGGAAAGATCTTGAGATGCTTCCCAGCCTGTTCACAGATCCCCTGG 3′
CY3-PCA3 Probe-C	5′ TCTAAACTCTTATAATCAAATTACACTTTTAGTATTTGCTGTCTC 3′
CY3-PCA3 pre-mRNA	5′ GAATAAAATTCCAAACCCATTCCCATGGCCTACAGACCTCTG 3′
CY3-GFP Neg Ctl	5′ ATGGAGAGCGACGAGAGCGGCCTGCCCGCCATGGAGATCGAGTGCCGCATCACCGGCAC 3′
CY5-PRUNE2	5′ CCAGGGGATCTGTGAACAGGCTGGGAAGCATCTCAAGATCTTTCCAGGGTTATACTTACTAGC 3′
CY5- GFP Neg Ctl	5′ TTACGTCGCCGTCCAGCTCGACCAGGATGGGCACCACCCCGGTGAACAGCTCCTCGCCCT 3′
Primers used for the synthesis of RNA probes	
T3BMCC1.fw	5′ ATCGAAATTAACCCTCACTAAAGGGAGCTGTCAGATGGAGAAATAAAAGTG 3′
T7BMCC1.rev	5′ ATCGATAATACGACTCACTATAGGGCACCAGGATCTCATCACAGCCA 3′
T3HESPCA3.fw	5′ ATCGAAATTAACCCTCACTAAAGGGTGGGAAGGACCTGATGATACA 3′
T7HESPCA3.rev	5′ ATCGATAATACGACTCACTATAGGGGAGGGTCCCTAGAGAGACACGAA 3′
T7GFP Neg ctl	5′ ATCGATAATACGACTCACTATAGGGGCTACTTGTACATTATTCTT 3′

Table S1. Cont.

Oligonucleotide ID	Sequence
Probes for Northern blot	
LNA-DIG PRUNE2 (NB-probe 2)	/5DigN/AGCAATCTGTCGTCTCGGCT/3Dig_N/
LNA-DIG BMCC1 (3′PRUNE2)	/5DigN/TATCCTGAATCTCCTCCGTGA/3Dig_N/
LNA-DIG PRUNE2 (5′ PRUNE2 NB-probe 1)	/5DigN/TGGTATGTTCAGCACTGGTAAA/3Dig_N/

ACTIN-DIG Probe Cytoplasmic RNA (Purchased from ROCHE).

Table S2. Primers for RT-PCR, PCR, cloning, and editing analysis of dsRNA *PCA3*/Intron6-*PRUNE2*

Primer name	Forward sequence (5′→3′)	Primer name	Reverse sequence (5′→3′)
Intron6-PRUNE2-1	AGAAGAAATAGCAAGTGC	PCA3-1	TCGGCTGCAGCCACACAA
Intron6-PRUNE2-2	GAAAACGATGCCATAGAA	PCA3-2	CATTCAAAACAATTGAC
Intron6-PRUNE2-3	GGTTGCAGTGAGCCAAGA	PCA3-3	TTTTTGAGGCAGAGTCT
Intron6-PRUNE2-4	TCTACCTCTCCCACCTCG	PCA3-4	GGCAAGGTTAAGATTTC
Intron6-PRUNE2-5	ATGGCTATTCTCATCTTC	PCA3-5	TCCTTGCTCTTTTACACC
Intron6-PRUNE2-6	ATTTAATCACAAATCACT	PCA3-6	TATTTTAATGTAGCATAG
Intron6-PRUNE2-7	GTGCTGAGATTACAGGCG	PCA3-7	CCTACAGAAATACAAGCA
Intron6-PRUNE2-8	GAAACTAACATTTCAACC	PCA3-8	ATTGTTGCAATAAACCTA
Intron6-PRUNE2-9	ACAATGAGGAAGACTACG	PCA3-9	AAAGTAGCCATTATTACC
Intron6-PRUNE2-10	TTGCTACGTAGTCTTGAA	PCA3-10	TGGTTTCCTTTAAGAGTT
Intron6-PRUNE2-11	AGAATGGGAAGAAAGGTT	PCA3-11	ATTACAGGAAGCCAGAT
Intron6-PRUNE2-12	CGATCCTCCCACCTGACCC	PCA3-12	AAAAATTAACTGGGCATG
Intron6-PRUNE2-13	AAGAAAGGACTTTTTCACT	PCA3-13	TCCCAAATTCTAAGACTC
Intron6-PRUNE2-14	AGACAATCTCACGTGCACA	PCA3-14	GCTTACTGTCTTTACTGA
Intron6-PRUNE2-15	ACTCAGCGGAGATTCTCGGC	PCA3-15	GGTGCAGTGGCAGATGTG
Intron6-PRUNE2-16	TGTTTTCTAGTCAGAGAGG	PCA3-16	CTAGAACACAGCAAGCAT
Intron6-PRUNE2-17	AACTGAGAAATGGCATAACA	PCA3-17	TATGAGATTGAATGATAA
Intron6-PRUNE2-18	TCCTGACTGTGGGCTCAGAT	PCA3-18	TGAAACATTCATTATCC
Intron6-PRUNE2-19	GTGAACCCAGGAGGCAGAGC	PCA3-19	GCTCTGTCGCCCAGGCTG
Intron6-PRUNE2-20	TAAACTTAAAAATTACTTTC	PCA3-20	TGTATATAACCTATTTTA
Intron6-PRUNE2-21	TTTTTACAGCCTTGGGAAAG	PCA3-21	GTAGTTGTCTTCATGTTTC
Intron6-PRUNE2-22	TATTGGCCAGGCTGGTCTTG	PCA3-22	CCCAGCACTTTGGGAGGCT
Intron6-PRUNE2-23	TCCTGTTGTGGATATTTATT	PCA3-23	ATTGGTAATGCTCACTTT
Intron6-PRUNE2-24	TAACTTGTAATTCCTTGAA	PCA3-24	AGAGACAAGGAAGAGCTT
Intron6-PRUNE2-25	AGCTGGGGCTGTGCATCAGG	PCA3-25	AGGGAATTCAAATTCTGG
Intron6-PRUNE2-26	CTTTACGTTCTGGGATAC	PCA3-26	CTTTACGTTCTGGGATAC
Intron6-PRUNE2-27	AGAAGCTGGCATCAGAAAAA	PCA3-27	CATTCAGTTAACAGTTTGGAAGG
Intron6-PRUNE2-28	TATGTGGGTTGGCATTCTTG	PCA3-28	TTTACGTTCTGGGATACATGTGC
Intron6-PRUNE2-29	GGGAAGGACCTGATGATACA	PCA3-29	CTGGAAATGTGCAAAAACAT
Intron6-PRUNE2-30	AGTCCGCTGTGAGTCT	PCA3-30	GCCTCAGATGGTAAAGTCAGC
Intron6-PRUNE2-31	ATCGACGGCACTTTCTGAGT	PCA3-31	CCCAGGGATCTCTGTGCTT
Intron6-PRUNE2-32	AAGAAAGGCTGCTGACTTTACCATCTGAGGC	PCA3-32	CCATTTCAGCAGATGTGTGG
Intron6-PRUNE2-33	CTGTGAACAGGCTGGGAAGCATCTCAAGATC	PCA3-33	AGATCCCTGGGAGAAATGCCCGGCC
Intron6-PRUNE2-34	CCGAGAAGCTGGCATCA	PCA3-34	GATCTTGAGATGCTTCCCAGCCTGTTCACA
Intron6-PRUNE2-35	GCTGCAGCCGAGGGAGAC	PCA3-35	TTTCAAATCTGTAATCCCGTTCAA
Intron6-PRUNE2-36	TGGTGGGAAGGACCTGATGA	PCA3-36	TTAAAGGGGCTGGAAATGTGC
Intron6-PRUNE2-37	CCTTCTGGGCCCAACATTCT	PCA3-37	GATCTTGAGATGCTTCCCAGCCTGTTCACAG
Intron6-PRUNE2-38	CCCATCCCTCCAGCCTTATC	PCA3-38	AGATCCCTGGGAGAAATGCCCGGCC
Intron6-PRUNE2-39	TCATGCAGTGCAAATCCCCA	PCA3-39	GCCCAGAAGGAACCGTAGAG
Intron6-PRUNE2-40	CCTCGCATTTGTGGGTTCTC	PCA3-40	TTTGCTTCACATCCCAGGCT
		PCA3-41	GAACCCACAAATGCGAGGTG
		PCA3-42	GGCCAGAAGCTAGCATCCAT
		PCA3-43	ACAAGGAGCCACTGGGTTTC